Interactions between low energy electrons and DNA

Kohanoff, J., McAllister, M., Tribello, G. A., & Gu, B. (2017). Interactions between low energy electrons and DNA: a perspective from first-principles simulations. *Journal of Physics: Condensed Matter*, *29*(38), 383001. https://doi.org/10.1088/1361-648X/aa79e3

Published in:
Journal of Physics: Condensed Matter

Document Version:
Peer reviewed version

Queen's University Belfast - Research Portal:
Link to publication record in Queen's University Belfast Research Portal

Interactions between low energy electrons and DNA: A perspective from first-principles simulations

Jorge Kohanoff [1*], Maeve McAllister [1], Gareth A. Tribello [1] and Bin Gu [1,2]

[1] Atomistic Simulation Centre, Queen's University Belfast, Belfast BT7 1NN, UK
[2] Department of Physics, Nanjing University of Information Science and Technology, Nanjing 21004, China

E-mail: *j.kohanoff@qub.ac.uk

March 2016

Abstract. DNA damage caused by irradiation has been studied for many decades. Such studies allow us to better assess the dangers posed by radiation, and to increase the efficiency of the radiotherapies that are used to combat cancer. A full description of the irradiation process involves multiple size and time scales. It starts from the interaction of radiation – either photons or swift ions – with the biological medium. Such interactions cause electronic excitation and ionisation. The two main products of ionising radiation are thus electrons and radicals. Both of these species can cause damage to biological molecules, in particular DNA. In the long run, this molecular level damage can prevent cells from replicating and can hence lead to cell death. For a long time it was assumed that the main actors in the damage process were the radicals. However, experiments in a seminal paper by the group of Leon Sanche in 2000 showed that low-energy electrons (LEE), such as those generated when ionising biological targets, can also cause bond breaks in biomolecules, in particular strand breaks in plasmid DNA [1]. These results prompted a significant amount of experimental and theoretical work aimed at elucidating the role played by LEE in DNA damage.

In this Topical Review we provide a general overview of the problem. We discuss experimental findings and theoretical results hand in hand with the aim of describing the physics and chemistry that occurs during the process of radiation damage, from the initial stages of electronic excitation, through the inelastic propagation of electrons in the medium, the interaction of electrons with DNA, and the chemical end-point effects on DNA. A very important aspect of this discussion is the consideration of a realistic, physiological environment. The role played by the aqueous solution and the amino acids from the histones in chromatin must be considered. Moreover, thermal fluctuations must be incorporated when studying these phenomena. Hence, a special place in this Topical Review is occupied by our recent first-principles molecular dynamics simulations that address the issue of how the environment favours or prevents LEEs from causing damage to DNA. We finish by summarising the conclusions achieved so far, and by suggesting a number of possible directions for further study.

Submitted to: *J. Phys.: Condens. Matter*

1. Introduction

DNA was discovered in 1869 by Friedrich Miescher. It then took about 50 years to identify the base, sugar and phosphate components that together form a nucleotide, and to determine that a DNA strand was simply a polymer of nucleotides connected through the phosphate groups. The first suggestion that genetic information should be encoded in a double-stranded molecular structure was made in 1927 by Nikolai Koltzoff [2], while the identification of this molecule as DNA was made by Avery, MacLeod and McCarthy in 1943 [3]. The precise determination of the structure of DNA in 1953 by Watson and Crick [4], using X-ray diffraction data obtained by Rosalind Franklin and Raymond Gosling, was the culmination of this massive body of research and remains the central pillar that underpins modern genetics. DNA contains the information used to synthesize the proteins that perform most cellular functions. This molecule is essential both in terms of inheritance and the cellular machinery of life. It is therefore not surprising that there has been a huge amount of research devoted to understanding the structure and function of DNA under varied circumstances.

1.1. DNA structure

The genetic information is stored in DNA as a code, which is written into its primary structure: the sequence of nucleobases. Each of the nucleobases in a DNA strand can only be one of the four nucleic acids Thymine (T or Thy), Cytosine (C or Cyt), Guanine (G or Gua), and Adenine (A or Ade). The first two of these bases are aromatic heterocyclic pyrimidines, while the other two are purines, which consist of a pyrimidine fused to an imidazole ring, as shown in Figure 1.

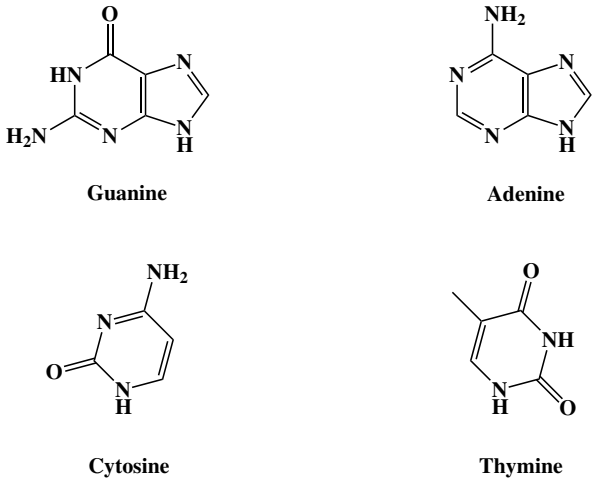

Figure 1. The four nucleobases present in DNA.

In the single-stranded molecule RNA, the role of thymine is played by Uracil (U), which differs from T only in that the methyl group is replaced by a hydrogen. DNA

nucleotides are composed of one of the four nucleobases above, a sugar component (deoxyribose) and a phosphate component (phosphoric acid) as shown in Figure 2. The base and the sugar are linked by the C-N glycosidic bond (**A** in Figure 3), while the sugar and phosphate groups are connected through the C-O phosphodiester bond.

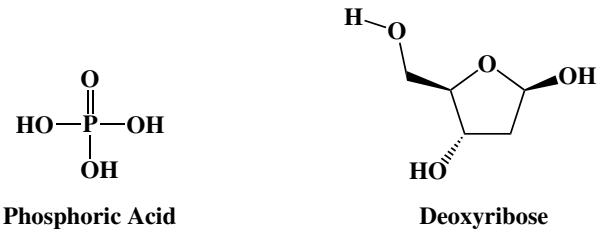

Figure 2. Phosphate and sugar components of a nucleotide

The backbone of DNA is built by connecting nucleotides via the phosphate group as shown in Figure 3. This introduces two types of phosphodiester bonds, the first of which is termed the $C_{3'}$-$O_{3'}$ bond, or simply the 3' bond. This bond is indicated using the letter **B** in Figure 3 and differs from the $C_{5'}$-$O_{5'}$ bond, or 5' bond, which is indicated using a **C** in Figure 3, as the carbon atom within it is part of the sugar ring.

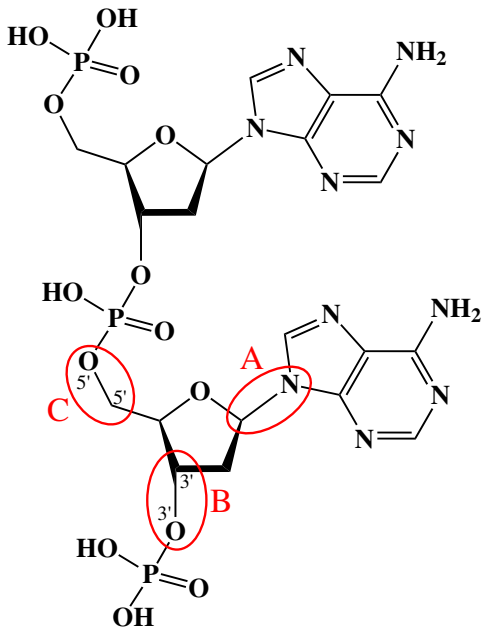

Figure 3. Adenosine dinucleotide showing the three components: base, sugar and phosphate, connected via glycosidic (**A**) and phosphodiester $C_{3'}$-$O_{3'}$ bonds (**B**). Consecutive nucleotides are linked through the phosphate component (the backbone) via a phosphodiester bond of a second type, $C_{5'}$-$O_{5'}$ (**C**).

When in vivo, DNA wraps around histone proteins to form chromatin, which in turn coils in the presence of the physiological medium that contains water, amongst other species. Chromatin is a macromolecular complex whose primary role is to package DNA

into a more compact shape. One of the roles of this compactification is to mitigate DNA damage. However, the structure of chromatin fluctuates as the cell cycle progresses, as it has to allow for DNA opening and replication during mitosis (cell division). At a genetic level, this complex is divided into chromosomes, which in turn are subdivided into nucleosomes containing around 150 base pairs. Figure 4 shows a view of a nucleosome, i.e. a basic unit of DNA consisting of a segment of DNA wound in sequence around eight histone protein cores, in a water background.

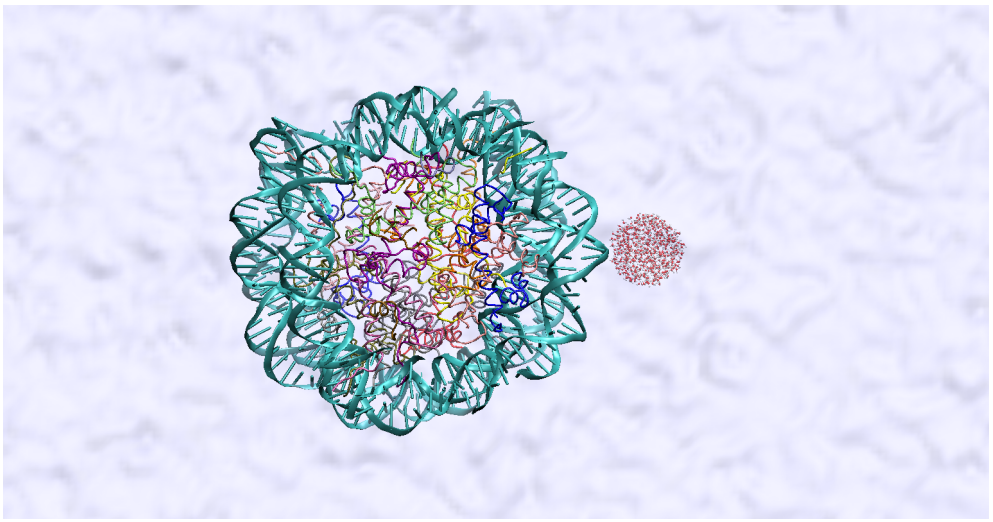

Figure 4. Nucleosome showing DNA in its physiological environment. DNA is wrapped around histones and solvated in water. The explicit water molecules shown in the figure represent the region affected by ionising radiation in an irradiation event. Figure created by P. de Vera, after E. Surdutovich, A.V. Yakubovich, and A.V. Solov'yov, Scientific Reports **3**, 1289 (2013).

This it not yet exactly the physiological environment, which should take into account the interaction of the nucleosome with other fragments of the wrapped chromatin. However, it is sufficient to highlight the main components in the DNA environment, i.e. water, RNA and proteins. In this review, following most of the theoretical work done so far, we will discuss the effects of radiation on DNA in model environments that capture the essential elements depicted in Figure 4.

1.2. DNA damage

Disruption of the DNA code leads to genetic mutations that can be more or less evidently expressed in observable characteristics of the individual. Such mutations are important in both normal (e.g. evolution) and abnormal (e.g. cancerous) biological processes. As well as mutations, which involve replacing one or more base pairs with others, the structure of DNA can also be damaged. Typical lesions of this type include: **(a) base excision**, i.e. the removal of a base by cleavage of the glycosidic bond, **(b) cross-linking**, i.e. the formation of inter- or intra-strand chemical bonds, and **(c) strand breaks** i.e. cleavage of the 3' or 5' phosphodiester bond. The most common strand

breaks are single strand breaks (**SSB**) in which there is only a break in one of the two strands of the DNA double helix. These breaks are particularly relevant in RNA or during replication of DNA, when the double helix opens for transcription purposes. A double strand break (**DSB**) is said to have occurred if both of the strands in a DNA double helix break and if the distance between the locations of the two breaks is less than ten base pairs.

The origin for either one of these types of damage can be natural, e.g. via metabolic processes. Metabolism releases, amongst other species, reactive oxygen, nitrogen and carbonyl species that can attack DNA. In the human body, such natural oxidative DNA damage events occur at a phenomenal rate of over ten thousand times per cell per day. However, damage can also be due to external influences, notably radiation. An excessive accumulation of damage in the DNA triggers, amongst other possibilities, what is known as *apoptotic* response, or programmed cell death. When the cell is not viable any longer because the genetic material is damaged, the reproductive cycle is arrested and the biochemical material is recycled.

If these damage processes were permanent, then there would be an inordinate amount of cells dying continually, and life as we know it would not be tenable. Nature, however, has developed a sophisticated enzymatic machinery to repair damage [5]. Interestingly, the instructions for building this machinery are also contained in the genetic code. Therefore, if those sections of DNA become severely damaged, then its ability to repair damage can be compromised. Repairing base excision and SSB is relatively simple, as the template remains intact. Repairing DSB is a different matter because the enzyme has to connect two separate pieces of DNA and *guess* how to do it properly without resorting to a template. The mechanisms by which enzymes repair DNA are varied, and constitute a field on its own, which has been recognised by the award of the 2015 Nobel Prize for Chemistry to Lindahl, Modrich and Sancar. Since metabolic damage is so common and independent of external sources, the enzymatic repair machinery is likely to be tuned for such processes. It is not clear, however, how effective this machinery is at repairing the damage induced by radiation. The two types of damage are not necessarily of the same nature, as the damaging agents are different.

1.3. Radiation damage of DNA

We will be concerned here with ionising radiation, i.e. ions or photons with energies above the ionisation threshold in biological systems, which is typically around 8.5 eV for nucleobases [6, 7] and 12.6 eV for water [8]. Biological matter is continually subject to ionising radiation. Some of this comes from natural sources such as UV-light from the sun, cosmic rays from space or from radioactive elements such as radon that can be present in soil and rocks, our blood and bones, and in the food and water we ingest. However, biological organisms are, in addition, voluntarily exposed to radiation sources such as medical X-rays and consumer products such as luminised watches and smoke detectors [9]. On average, the equivalent radiation dose – a measure of the biological

effect – absorbed annually by humans is about 2.4 mSv. The official recommendation is that any exposure above the natural background radiation should be kept below 1 mSv per year. However, background radiation is not uniform, and there are regions in the world where it is significantly higher than the safety limit [9]. Furthermore, in space missions at the International Space Station, the typical equivalent radiation dose absorbed, mostly from cosmic rays, ranges between 50 and 2000 mSv. Understanding the effect this radiation has upon us is of paramount importance in terms of curing and preventing diseases such as cancer. Furthermore, if we truly want to minimise the biological effects of radiation, we need to have an understanding of the intricacies of the processes that lead to such damage. To achieve this, we need to focus our research on obtaining a solid understanding of how these processes operate at the atomic and molecular level. This is doubly true when delivering radiation such as photons, electrons from β-emitters, or ions [10] in a controlled manner for therapeutic uses.

Any of the components in a biological medium can be ionised, be they DNA, proteins, water or membranes. DNA – the molecule that encodes genetic information and that is responsible for cell replication and protein synthesis – is considered to be particularly sensitive to damage. DNA dysfunction can cause cell death through necrosis or the relatively benign process of apoptosis. Worse still, if DNA damage disrupts normal cellular processes such as apoptosis, cell replication can become uncontrolled and cancerous tumours can begin to form.

There are two main ways radiation can cause damage to DNA. One of them is *directly*, by ionising DNA and creating electron *holes* that weaken the backbone as part of a process that can cause strand breaks. The other one is *indirectly*, and is initiated by the ionisation of the surrounding medium, i.e. water, proteins, etc. Any incident radiation will interact with these components generating *secondary* species, namely electrons and radical cations, i.e. molecules with a missing electron (or containing a *hole*), both of which can go on to attack DNA. One might argue that questions of what percentage of damage can be attributed to direct radiation and what percentage can be attributed to indirect radiation are the most fundamental in setting research priorities.

It is tempting to argue that the amount of DNA in the nucleus and the mitochondria of the cell is insignificant when compared to the amount of other material in the cell. One would thus expect indirect damage to be a much more important pathway as any radiation will most likely encounter the molecules in the medium rather than the DNA. While the proportion of direct to indirect damage depends on the type and energy of the radiation, experimental evidence suggests that the environment is responsible for approximately 66% of the damage [11, 12]. An explanation for this large, but not overwhelming contribution is that, for an ionisation event to lead to DNA damage, it has to occur relatively close to the DNA. An estimate based on the mean free path of electrons in water suggests that only ionisation events occurring within a region between 1 and 10 nm from the DNA can contribute to the damage [13]. In the case of radicals, their contribution is controlled by their diffusion properties in the medium. Typical diffusivities of $OH^{\bullet}$ in water are of the order of 3×10^{-9} m^2/s, i.e. similar to water self-

diffusion [14]. These values are not too large, but in the case of ion irradiation, they can be boosted by the rarefaction wave (shock wave, for heavy ions) driven by the ionisation of the material in the surrounding of the ion track [15, 16]. These considerations lead to the following central questions:

- How does the ionisation of the medium cause DNA damage?
- Do all ionisation products generated in the medium interact with DNA and cause damage, or do only a fraction of them do this?

In answering these questions we must investigate the transport properties of the medium and its reactivity. That is to say we have to determine how fast and far these products travel, and what happens to them when they stop in the medium. In particular, does their stopping reduce their reactivity, inactivate them and prevent them from causing further damage? This review will focus on indirect damage but, for completeness, we briefly mention some interesting aspects of direct damage.

1.3.1. Direct damage. The consequences of direct damage, i.e. the dynamics of holes in DNA, was studied intensely in the late nineties and onwards. It was rapidly established that holes can travel long distances [17, 18], via a hopping mechanism between trapping sites. Trapped holes couple to lattice distortions forming polarons [19], and preferentially localise in guanine-rich regions, although they appear to be delocalised over a few bases rather than on a single one [20]. Furthermore, there is unequivocal evidence that single and double strand breaks occur in DNA that contains holes [21]. In this review we will not discuss holes in DNA, but it is worth mentioning that the discovery of high hole and electron conductivity through DNA prompted a significant amount of research exploring potential applications in other fields such as molecular electronics, with recent reports suggesting that this may become a reality in the coming years [22].

1.3.2. Indirect damage. When in vivo, DNA wraps around proteins to form chromatin, which in turn coils in the presence of water, as shown in Figure 4. Any incident radiation will thus interact with proteins and water, ionising them and generating *secondary* species, essentially secondary electrons and reactive radicals.

High-energy electrons, i.e. those arising from the tail of the distribution, interact with the medium via electron impact ionisation and so generate secondary electrons while losing a fraction of their kinetic energy. These secondary electrons also undergo collisions producing tertiary electrons, and so on. The overall result is a radiation cascade in which most of the secondary, tertiary, and further electrons end up having energies under $\approx$ 30 eV. The species that result from this process are the so-called *low-energy electrons* (LEE) [11], and follow an energy distribution that peaks at about 9-10 eV, as shown in Figure 5 [23]. LEE diffuse through the medium polarising it and interacting inelastically with the molecules of which it is composed, e.g. water, proteins, etc. As a result of these interactions LEE lose energy by transferring it to electronic and vibrational excitations of the molecules in the medium. Through this process, LEE

slow down, and the majority of them become thermalised, solvated electrons in a time scale on the order of ps. However, along their way they generate a wealth of potentially damaging species that are described in what follows.

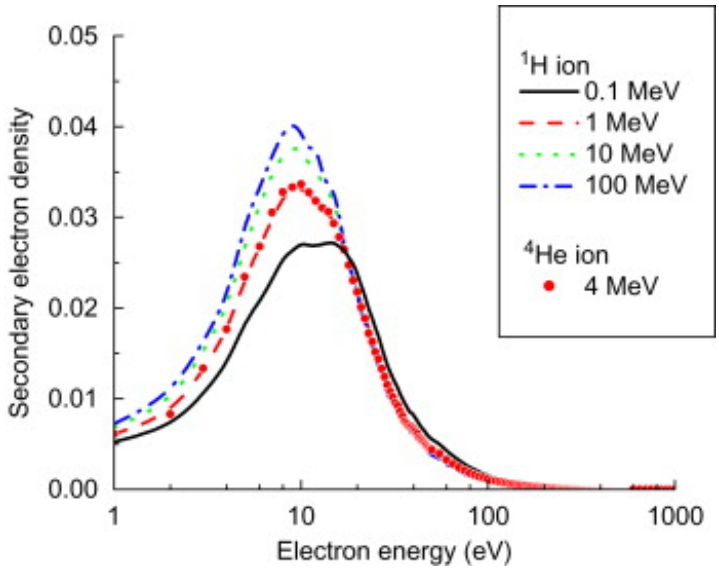

Figure 5. Energy distribution of secondary electrons produced by swift protons of various energies, and He ions in water. Notice the mild dependence of the distribution on the energy of the projectile. Reprinted from S. M. Pimblott and J. A. La Verne, Radiat. Phys. Chem. **76**, 1244 (2007), Copyright 2007, with permission from Elsevier.

When radiation interacts with water the following chemical reaction occurs:

$$H_2O + \textit{radiation} \rightarrow H_2O^{\bullet +} + e^-_{aq} \ , \tag{1}$$

In the above the e^-_{aq} is used to represent the hydrated electron and the bullet indicates that the H_2O^+ ion is a radical, i.e. a molecule with a partially filled electronic shell. The two products of the above reaction can react with water as shown below:

$$e^-_{aq} + H_2O \rightarrow H^{\bullet} + OH^- \tag{2}$$

$$H_2O^{\bullet +} + H_2O \rightarrow H_3O^+ + OH^{\bullet} \ . \tag{3}$$

Reaction (2) is supposed to be slow, which is why it is widely assumed that, when electrons solvate in water and become hydrated electrons, their reactivity drops and their potential to induce DNA damage is reduced significantly. *As a consequence, DNA damage has been traditionally assumed to involve the radicals and not the electrons.* Experimental data, however, shows that, in solution, nucleobases are indeed reduced by solvated electrons [24]. Very recent theoretical calculations support this notion and also estimate a time scale between 10 and 120 fs for the reaction assuming that the e^-_{aq} and the base are in close proximity of each other [25]. This reaction is then limited by the diffusion of the two species relative to each other.

In contrast to reaction (2), reaction (3) is very fast and represents the main source of hydroxyl radicals ($OH^{\bullet}$), which can also be formed by the dissociation of excited

water molecules into $OH^\bullet$ and $H^\bullet$. Hydrogen radicals react with each other to form H_2, while two hydroxyl radicals can react to produce hydrogen peroxide [26]. The two most important mechanisms by which $OH^\bullet$ radicals attack DNA are by adding themselves to the π bonds of DNA bases, or by abstracting a hydrogen atom from the sugar component. Both of these reactions are fast in contrast to reactions between $OH^\bullet$ and phosphate [27]. Therefore, strand breaks due to $OH^\bullet$ proceed mostly via indirect mechanisms [27].

The two radiolysis products from reaction (1), i.e. $H_2O^{\bullet+}$ and e^-_{aq} can also react directly with DNA as shown below [28]:

$$e^-_{aq} + \mathrm{DNA} \rightarrow \mathrm{DNA}^{\bullet-} \tag{4}$$

$$H_2O^{\bullet+} + \mathrm{DNA} \rightarrow \mathrm{DNA}^{\bullet+} + H_2O\ , \tag{5}$$

The second of these two reactions involves the radical water cation once more and thus competes with reaction (3). As reaction (3) is very fast and as water is much more abundant that DNA, the majority of the radical water cations are transformed into $OH^\bullet$ radicals, and do not attack DNA directly.

Another reactive channel that avoids electron solvation altogether is the resonant trapping of electrons by the molecular potential at specific, well-defined, positive energies. When an electron attaches resonantly to molecule A, it forms a transient negative ion (TNI) A^{-*}, where * signifies that this species is in a excited state. Resonances are not strictly stationary states in the quantum-mechanical sense. They have a lifetime after which they undergo the reaction $A^{-*} \rightarrow A + e^-$. The narrower the resonance is in energy, the longer the lifetime, and vice versa. In a TNI the electronic degrees of freedom are coupled to the vibrational motion of the molecule. Consequently, there is a non-negligible probability for the electronic system to decay into a lower-lying electronic state of the molecule while transferring energy into the vibrational motion of specific bonds. If the amount of energy transferred to vibrations during this process is sufficiently large, this can cause bond cleavage and the trapping of the electron in a bound state of the molecule (at negative energy). This process is known as *dissociative electron attachment* (DEA) and is known to occur when LEE interact with water molecules. A resonance at an energy of about 7 eV [29], leads to the formation of an $OH^\bullet$ radical and a hydride anion via the reaction:

$$H_2O + e^- \rightarrow H_2O^{\bullet-} \rightarrow OH^\bullet + H^-\ . \tag{6}$$

In summary, the two main water radiolysis products are the $OH^\bullet$ radicals that are generated through reactions (3) and (6), and the electrons which are generated through reaction (4). Both of these radiolysis product can damage DNA and, in the long run, this damage can prevent cells from replicating and thus cause cell death. For a long time it was assumed that the radicals were the main actors in this process. However, in 2000 experiments reported in a seminal paper by the group of Leon Sanche in Sherbrooke showed that LEE can also cause strand breaks in plasmid DNA [1]. While $OH^\bullet$ and other radicals remain an important source of damage, this is closer in nature to metabolic

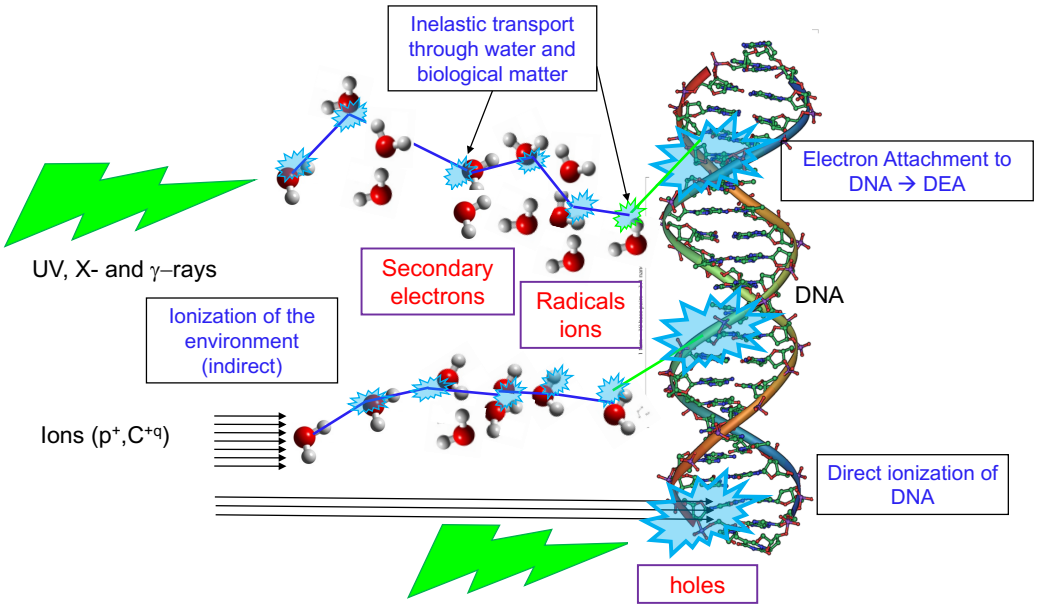

Figure 6. Schematic representation of the processes involved in the interaction of radiation with biological matter.

damage and is therefore likely to be easier to repair. Figure 6 summarises schematically the types of DNA damage due to ionising radiation.

In this review we explore the damage secondary electrons can do to DNA and focus on the interactions between LEE and DNA, and the manner in which such interactions lead to DNA damage. The results presented in Ref. [1] motivated a large amount of both experimental [11, 30, 31, 32, 33] and theoretical [34, 35, 36] work that aimed at elucidating the role played by LEE in DNA damage. In recent years, this research has moved on from idealized systems, e.g. isolated DNA components in either the gas phase or a microsolvated environment, towards a more realistic model for the environment that better represents the physiological one. Incorporating these more accurate models for the environment requires one to take both the aqueous solution containing the ions and the presence of amino acids from the histones in chromatin into account. Moreover, incorporating thermal fluctuations is essential, as all processes happen at room temperature. Understanding DNA damage under these conditions constitutes a fundamental step towards a thorough assessment of the dangers posed by involuntary exposure to radiation. It also enables a finer control of radiotherapeutic treatments of cancer, and the development of new, more efficient and less harmful radiotherapies.

1.4. DNA damage by low-energy electrons

LEE generated by water radiolysis can be captured by DNA and form the transient anion $DNA^{\bullet -}$. Much like water, $DNA^{\bullet -}$ can dissociate via DEA, using the excess electronic energy to break specific bonds. The first experiments that detected DNA

damage at low electron energies, and that therefore probed the DEA mechanism, were conducted by Leon Sanche's group in 2000 [1]. Prior to this work, electrons had only been observed to cause DNA damage when they had energies above 30 eV. This was one of the reasons why $OH^{\bullet}$ radicals were believed to be the key agent in indirect DNA damage [26]. The observation that LEE could cause damage is particularly significant, because electrons are as or more abundant in irradiated cell conditions than radicals [37]. In Sanche's experiments, plasmid DNA was irradiated with electrons with well-defined incident energies that ranged from 3 to 20 eV. The number of DNA strand breaks per incident electron was measured using the gel electrophoresis technique. This technique works because undamaged DNA, DNA containing SSB, and DNA that contains DSB, have different shapes and sizes, and hence travel at different speed through the gel under the influence of an applied electric field. This allows for a quantitative evaluation of the different types of damage [38]. A main finding is that the amount of DNA damage does not grow monotonically with energy, but exhibits an interesting structure, as shown in Figure 7.

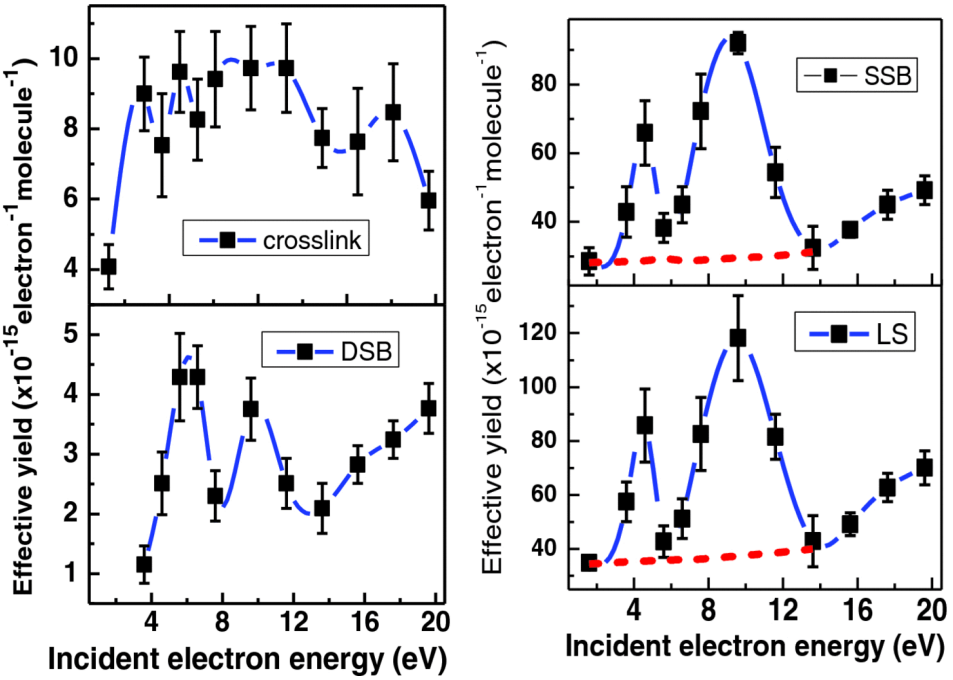

Figure 7. DNA damage yields caused by low energy electrons. Peaks observed at energies in the 7-10 eV range are ascribed to resonant behaviour, leading to dissociative electron attachment. These resonances fall in the same region of those in water. Reprinted from X. Luo, Y. Zheng, and L. Sanche, J. Chem. Phys. **140**, 155101 (2014), with the permission of AIP Publishing.

Figure 7 reports the yields of crosslinks, SSB, DSB, and loss of supercoiled configuration, as a function of the incident electron energy, [39] and expands on the original results reported in Ref. [1]. This figure shows a large number of lesions are observable at energies lower than the ionisation potential of DNA, which is between

7.5 and 10 eV across the four nucleobases [40]. This suggests a low energy mechanism at play. The authors argued that this mechanism was dissociative electron attachment leading to the cleavage of the phosphodiester bond - a process which manifests itself as a strand break. This hypothesis was soon supported by Barrios *et al* [41] who showed, using first-principles calculations, that the excess electron is captured in a π^* orbital located in the nucleobase, and transferred remotely to the phosphodiester bond due to the electron-vibration coupling. A few years later Sanche's group extended their experiments to lower energies and showed that strand breaks can occur even when the electrons have very low energies, between 0 and 4 eV [42]. They observed strand break yield peaks at 1 eV and 2.5 eV (See Figure 8) and supported these observations with cross section calculations that further reinforced the DEA picture.

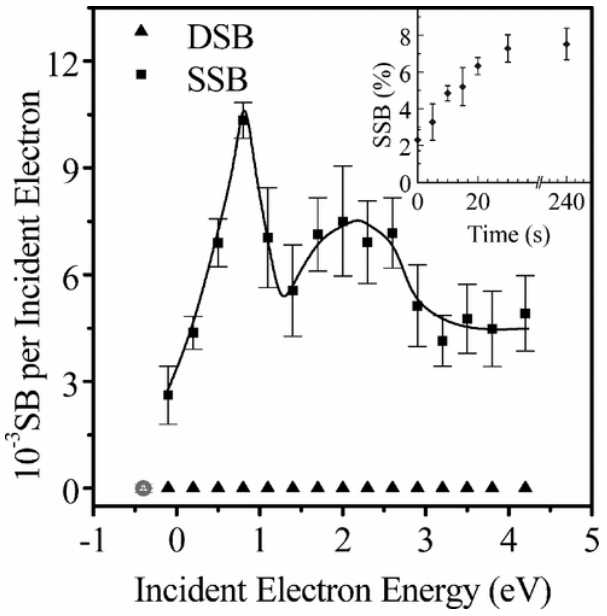

Figure 8. The peak/valley distribution of SSB is still observed at even lower energies (0-4 eV), with peaks observed at 0.8 eV and 2.2 eV. DSBs are not observed at such low energies. Reprinted with permission from F. Martin *et al* , Phys. Rev. Lett. **93**, 068101 (2004). Copyright 2004 by the American Physical Society.

1.4.1. Electronic resonances in DNA subunits. The connection between resonant energies in DNA and capture in the nucleobases was corroborated by comparing to earlier gas phase experiments by Huels *et al* [43], in which a molecular beam of the DNA bases was made to interact with an electron beam. An analysis carried out by mass spectrometry to identify ion signals clearly revealed two low-energy resonances, one at around 1 eV, and the other in the range 6-12 eV. There are thus two major types of transient negative ions (TNI) formed via LEE attachment to DNA subunits (nucleobases, sugar or phosphate components) that can lead to damage [33]:

(i) *Shape resonances*, in which the electron temporarily occupies a previously empty orbital of a DNA subunit and is trapped by an angular momentum barrier. At low energies the TNI will exist for long enough for DEA to occur [44] but, at higher energies, the quasi-bound electron will tunnel so rapidly that it will escape the molecule before DEA can take place [45].

(ii) *Core-excited Feshbach resonances*, in which the electron is captured in an electronically excited state of the DNA subunit. The molecule will eventually decay in to the parent state, but Feshbach resonances are generally quite sharp and hence longer-lived than lower energy shape resonance. Furthermore, they carry a larger damaging potential because a larger energy is available for transfer to vibrations [34].

Gas phase experiments [43, 46, 47, 48, 49, 50, 51, 52] revealed that below the electronic excitation energy level (3-4 eV), the TNI that are most likely to form are shape resonances of the basic subunits of DNA. At higher energies the TNI formed are Feshbach resonances.

1.4.2. Dissociative electron attachment (DEA) in nucleobases. The pathway via which a TNI dissociates depends on the resonant energy at which it is formed. In all these pathways, the excess energy of the attached electron transfers through the molecule causing the dissociation of a bond that may well be quite distant from the region where the electron attaches. Crossed-beam collision experiments on each of the four nucleobases found that low-energy resonances dissociated via the loss of a neutral hydrogen atom [50], leaving a dehydrogenated negative ion $[\text{Thy-H}]^-$. Extensive studies of the Thymine nucleobase [51] found that, at typical shape resonance energies (0-3 eV), there was an interesting energy-dependent bond selectivity. For example, N1-H cleavage resulted from a 1 eV resonance, while at 1.8 eV, cleavage was observed in the N3-H bond (see Figure 9 for the locations of these bonds). When the TNI was formed at the higher energy resonance (6-12 eV), the prominent reaction was the release of a hydride H^- ion, leaving a neutral $[\text{Thy-H}]^\bullet$ radical. This reaction was observed to extend over the whole resonance region [51].

The transient negative ion is a challenging species to investigate, precisely because it is metastable and relatively short-lived. One way to identify them experimentally uses crossed-beam scattering experiments in which the energy of the incident electron beam is scanned over the desired energy region. Peaks in the cross section correspond to DEA resonances, and can be measured via mass spectrometry of the fragments detected in the exit channel. In DNA, such peaks are observed in the region 0-10 eV [53].

From the theoretical side, several methodologies have been developed to compute scattering cross sections. Most of the work on biomolecules and DNA subunits has been carried out using R-Matrix theory. In R-matrix theory, the scattering center, e.g. a molecule, is enclosed in a spherical region inside which the electronic structure is determined to a high accuracy, typically at the configuration interaction level. The

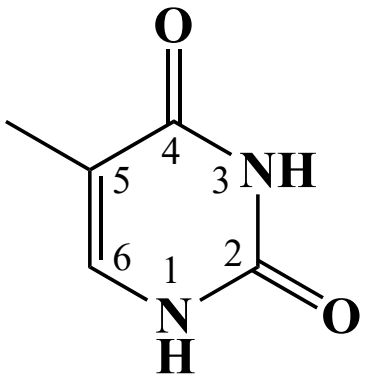

Figure 9. Thymine base with ring atoms numbered. When a 1 eV electron forms a TNI with it, cleavage occurs at the N1-H bond. At 1.8 eV, cleavage is observed at the N3-H bond [51].

internal wave functions are then matched at the surface of the sphere with external incoming and outgoing waves, which are expanded in partial waves. The enforcement of such boundary conditions, similarly to the case of scattering by a one-dimensional potential well, determines the scattering cross section as a function of energy. This methodology has plenty of numerical subtleties. One of the most important ones being a need for (pseudo-)states in the continuum that correspond to scattering, rather than to bound states of the potential. A second, very important choice is the basis set that is used to represent the wave functions inside the sphere. For atoms it is more or less straightforward, but for molecules one is faced with the question of whether to use a single-center or a multi-centre expansion. Both have their advantages and disadvantages. A thorough review of R-matrix theory and applications to molecular resonances can be found in Ref. [54]. This formalism considers fixed nuclei, which is not appropriate to the computation of DEA cross sections, where the electronic and nuclear dynamics are coupled. Extensions of R-matrix theory that include nuclear dynamics have been proposed by Fabrikant [55] and Domcke [56], amongst others. The quasi-classical approach of Fabrikant uses *ab initio* potential energy surfaces (PES) and resonance widths as a function of nuclear geometry as input data for the computation of DEA cross sections. This formalism is suited for the excitation of a single vibrational degree of freedom, which works well for diatomic molecules, but in a more general context, it requires the freezing of all but one vibrational degree of freedom. More general schemes that use multi-dimensional PES have also been proposed [57]. The theoretical description of the coupled electron-nuclear dynamics as it occurs in DEA remains a challenge. Some alternative ideas will be discussed in Section 2.

Caron and Sanche investigated low energy resonances in DNA using R-matrix calculations for the atomic centres combined with a multiple scattering approach to take into account the molecular environment [58]. In this way they calculated cross sections for large, model helical DNA structures, and predicted resonances that were below 15 eV and which would contribute to an explanation for the stand breaks observed

in experiments. A more accurate determination was provided later using a similar approach, but using collisional data for DNA subunits instead of atomic data [59].

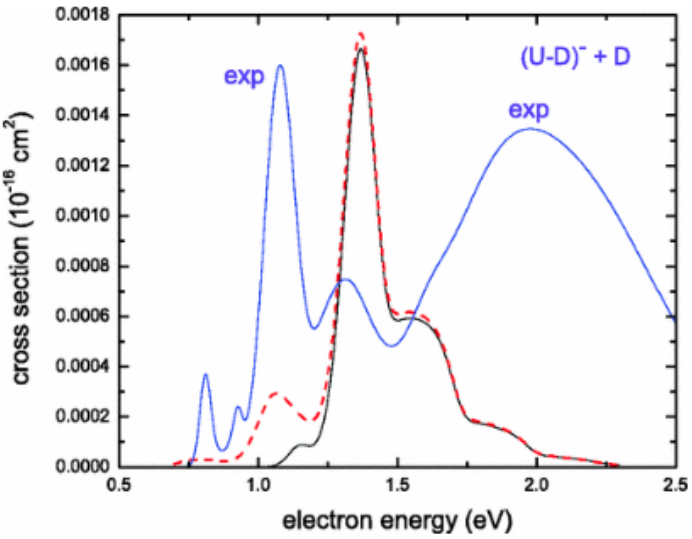

Figure 10. Cross-section for DEA of Uracil at N1-H comparing R-Matrix theory results with experiment. The height and shape of the calculated cross-section (black line) is in good agreement with experiment (blue line). The experimental peak however occurs at an energy 0.27 eV lower than the R-Matrix peak. Reprinted with permission from G. Gallup and I. Fabrikant, Phys. Rev. A **83**, 012706 (2011). Copyright 2011 by the American Physical Society.

During the DEA reaction the electron decays into a bound state while releasing its excess energy and causing dissociation. The cross section energies represent the excess energy that will be used to excite bond vibrations and thus make bonds prone to cleavage. DEA cross sections can be calculated using R-Matrix theory, as shown by Gallup and Fabrikant [60], who investigated the dissociation of uracil. Using a finite element discrete model [61], they calculated the PES for the TNI corresponding to LUMO of *a1* symmetry. This resonance is very broad at the equilibrium nuclear configuration, but becomes narrower when the N1-H bond is stretched, eventually leading to the formation of a stable $[U\text{-}H]^-$ ion. The nuclear dynamics was then included using the R matrix theory, and a pronounced vibrational Feshbach resonance [62] was found near the DEA threshold, see Figure 10. The position of this resonance, 1.4 eV, is somewhat above the experimental peak value, 1.1 eV, but overall shape of the curve is very well reproduced.

These are gas-phase results. It is not quite clear what are the implications for more representative environments, e.g. when the base is solvated in water. In order to start answering this question, Smyth *et al* extended the previous work by supplementing R-matrix calculations with multiple scattering theory to take the effect of microsolvation, i.e. the presence of a small number of water molecules hydrogen-bonded to Uracil, on

the DEA process into account [63]. A first finding was that the N1-H resonance shifted towards lower energies due to the stabilising role of the environment. More importantly, the width of the resonance peak reduced, thus increasing the lifetime of the resonance and enhancing the DEA cross section by a factor six, as shown in Figure 11. This suggests that dissociation of $[\mathrm{Thy}]^-$ is more likely in an aqueous environment than it is in the gas phase.

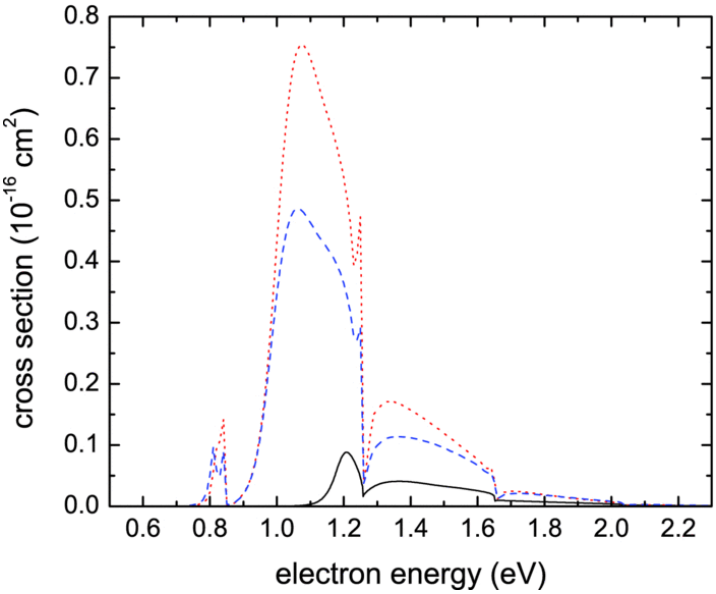

Figure 11. DEA cross section for Uracil: isolated (black solid line) and embedded in the $(H_2O)_5$ cluster. The location of the resonance is shifted by $\Delta E = -0.326$ eV. The dotted red curve is the cross section calculated with inclusion of scattering by all molecules in the cluster, while the dashed blue curve considers scattering from water molecules. Reprinted from M. Smyth, J. Kohanoff, and I. Fabrikant, J. Chem. Phys. **140**, 184313 (2014), with the permission of AIP Publishing.

1.4.3. DEA in other DNA subunits: sugar, phosphate, nucleosides and nucleotides. So far we have only reviewed work on the DEA of nucleobases. We have established that low-energy electrons (0-10 eV) are likely to be captured resonantly leading to dissociation via cleavage of the N-H bonds. This phenomenon, however, is not directly relevant to the strand breaks observed in Sanche's initial work on plasmid DNA [1, 42] as strand breaks are associated with the cleavage of the phosphodiester C-O bonds between sugar and phosphate that hold the DNA strand together - the bonds labelled B (3') and C (5') in Figure 3. Instead, the cleavage of bond A, i.e. the glycosidic C-N bond, leads to base excision.

The sugar moiety in the gas phase also displays resonant attachment properties, but it is less likely to attach an electron and decay than a nucleobase. Studies of electron attachment to an isolated sugar found two resonant features. One at 0 eV, and a broader resonance at 6-9 eV. These resonances decay via the loss of one or more

neutral water molecules and CH_2O molecules [64, 65, 66] and the associated reactions are more complex than the dehydrogenation of the nucleobases. Quantum dynamics scattering calculations [65], confirmed that shape resonances in the ribose should not exist at 0 eV but will be produced between 7-10 eV. The dissociation that is observed at 0 eV is thus still unexplained. However, when the sugar is bound to the nucleobase, as in a nucleoside, DEA is likely to occur. This was observed by Ptasinska *et al* , who performed thermal evaporation experiments on Thymidine [67, 68]. At energies below 3 eV, the molecule exhibited two resonances: the cleavage of the glycosidic bond at 1.2 eV, and a shape resonance at 1.8 eV on the nucleobase, which resulted in a release of the N3-H hydrogen.

The investigation of the isolated phosphate unit as it appears in a DNA nucleotide is experimentally difficult. One possibility is to use phosphoric acid derivatives bound to hydrocarbons as was done by Konig *et al* [69]. They used $(C_4H_9O)_2POOH$ because of its closeness in structure to DNA. In terms of DNA damage, the most significant reaction was the C-O bond cleavage, which is equivalent to a strand break. This reaction took place in two broad resonances at 2-4 eV and 7-10 eV [70]. Electron attachment to the sugar-phosphate complex was also shown to lead to dissociation in the gas-phase by Bald *et al* , who used laser-induced acoustic desorption techniques [71]. This technique was used to transfer intact neutral biomolecules into the gas phase where they can interact with an electron beam. In this study, the ribose-5'-phosphate formed a TNI at 0 eV which resulted in cleavage of either the C-O bonds.

We can thus conclude that, of the individual building blocks of the DNA nucleotide, the nucleobase is the most sensitive to low-energy electron attachment. The base-sugar and sugar-phosphate components are sensitive to DEA and the bonds which can break in longer strands of DNA are the $C_{3'}$-$O_{3'}$ (B) or $C_{5'}$-$O_{5'}$ (C) phosphodiester or the C-N (A) glycosidic bonds shown in Figure 3, above. Soon after the original low-energy electron experiments by Sanche's group, Barrios *et al* [41] proposed the following mechanism for SSB. A low-energy electron ($\approx$ 1 eV) attaches to a π^*orbital of a DNA base to form a shape-resonance. This anion then undergoes a sugar-phosphate C-O bond rupture over a small barrier to produce a SSB. These authors also suggested that solvation should play a crucial role in the rate of SSB formation by stabilising the anion, which otherwise will be very short-lived against auto-detachment.

This mechanism has been revisited many times, e.g. [72, 73], but mostly from the point of view of ground state electronic structure calculations, which will be reviewed later. Full scattering R-Matrix calculations have been performed for systems as large as single DNA nucleobases in vacuum [74, 75], and microsolvated by up 5 water molecules [76]. This is practically the state-of-the-art for the calculation of electronic resonance cross-sections, while for DEA probably the largest system studied is the one in [63]. Theoretical and experimental progress in DEA has been reviewed very recently [77].

In what follows we will discuss the *post-DEA behaviour of DNA subunits* after the excess energy of the attached electron has been transferred to vibrations. The aim is to predict the likelihood of the reactions that could result from TNI decay

in different environments, from gas-phase to full solvation, as opposed to thermally-activated, electronic ground-state reactions.

2. Modelling the dynamics of DEA

The process of energy transfer from electronic excited states to vibrational motion is a typical example of non-adiabatic dynamics. Several methodologies have been developed during the past decades to describe such phenomena. It is not the aim of this review to discuss them in detail, but since this is one of the methodological frontiers, we will mention here some of these approaches.

First of all, the description of the electronic subsystem requires one to account, reasonably accurately, for excited states. This rules out immediately approaches such as standard DFT. While originally formulated as a ground state theory DFT, in principle, also allows for the determination of excited states. Formally, the electronic density determines univocally the external potential that leads to it, and this potential in turn determines the full many-body wave function, which includes excited states. Determining the wavefunction in this way is, however, not a practical recipe. Instead, it has been customary to identify the energy difference between empty and occupied Kohn-Sham, one-electron eigenstates as excitation energies of the many-electron system. The most prominent example is that of the HOMO-LUMO gap in molecules, or similarly the valence-conduction band gap in bulk semiconductors and insulators. This interpretation as excitation energy is often criticised by stating the the Kohn-Sham eigenstates are "meaningless" as these correspond to a fictitious, non-interacting reference system. However, it has been shown that this is a well-defined approximation to true excitation energies [78], and its quality depends on the exchange-correlation functional used. In addition, it is nowadays possible to compute electronic excitation energies in terms of one-electron eigenvalues to a very good accuracy using hybrid functionals that combine standard DFT approximations, such as the GGA, with Hartree-Fock exchange [79]. Quantum chemical methods also provide good estimates of excitations energies, but not at the Hartree-Fock (single-determinant) level. The lowest acceptable level is configuration interaction including single excitations (CIS).

An alternative to the methods described in the previous paragraph is to use time-dependent DFT (TDDFT), either in the frequency domain via linear response, or in real time. For finite systems such as molecules, standard TDDFT approximations such as the adiabatic GGA (AGGA), which is local in time and semi-local in space, corrects the DFT excitation energies quite well, unless they are of the charge-transfer type. For extended systems, however, the correction is diluted and becomes ineffective. Interestingly, TDDFT has been demonstrated in the computation of cross sections for electron-atom scattering [80]. This may be a read to explore in the near future, as TDDFT allows for the study of much larger systems than the quantum chemical approaches that are typically used in traditional scattering theory (CI).

The second aspect to take into account is the correlated motion of electrons and

nuclei. The combination of ground-state DFT for electrons with Newtonian dynamics for the (classical) nuclei has been an extremely valuable tool in the study of materials and biological systems. When using this technique the electrons are maintained in the ground state corresponding to the instantaneous nuclear configuration, and hence have no independent dynamics. This methodology relies on the separation of electronic and nuclear time scales, which is rooted in the Born-Oppenheimer approximation. The numerical integration of this scheme receives the name of Born-Oppenheimer molecular dynamics (BOMD), although it is sometimes called first-principles MD (FPMD), quantum MD (QMD) or ab initio MD (AIMD). The so-called Car-Parrinello molecular dynamics (CPMD) also falls within this class of methods, but it is implemented in a way that resorts to a fictitious dynamics for the electronic degrees of freedom [79]. In this sense, it is a precursor to methods that treat the electronic wave function or density as a dynamical variable, with the aim of re-introducing a proper independent electronic dynamics. The cost of this approach is to reduce significantly the integration time step, typically by a factor of thousand, thus compromising the ability to follow the nuclear dynamics in the same simulation, unless the system size is reduced significantly or inexpensive approximations to the electronic structure are used, such as simple model hamiltonians. Of course, it is possible to improve this description by resorting to higher-level approaches such as tight-binding (TDTB), quantum chemistry methods (e.g. TDHF), or TDDFT. Model hamiltonians are good for developing new methodologies [81], while tight-binding models, especially the so-called density-functional tight-binding (DFTB) approach, has proved useful for describing electron dynamics in large systems [82, 83].

Introducing the nuclear dynamics also requires approximations for the electron-nuclear correlation. The simplest one is to evaluate the forces on the atoms in correspondence with the time-evolving electronic density. In this approach the dynamics of the electronic density follows the von Neumann equation which, within TDDFT, is equivalent to integrating the time-dependent Kohn-Sham equations. This is called the *Ehrenfest* approximation, and it is essentially a mean-field approach in which the individual nuclei see the electrons through their density, but not individually. While electronic excitation processes are captured correctly by this approach [84], the mean-field character of Ehrenfest distorts the characteristics of energy transfer from electrons to phonons, e.g. Ehrenfest cannot describe properly ubiquitous phenomena such as Joule heating [85] or the thermalisation between electronic and nuclear degrees of freedom [81]. A second limitation is related to the exchange-correlation approximations used in TDDFT. In most cases, these are semi-local in space and local in time. Therefore, memory effects in the electronic evolution are ignored, which leads to another whole host of pathologies, mainly related to the lack of electronic decoherence (no electron-electron collisions term) [86]. In addition, incoherent electron-phonon scattering by nuclear vibrations (phonons), which are not explicitly represented in classical molecular dynamics, are not accounted for in Ehrenfest simulations [87]. While Ehrenfest dynamics is straightforward to implement and computationally efficient, it is not trivial to go

beyond it.

To improve on the electron-nuclear correlation, a possibility that has attracted interest is *surface hopping* [88]. In this method the forces on the nuclei are determined from single electronic potential energy surfaces (PES) but hops between surfaces are allowed in order to include non-adiabatic effects. Surface hopping works reasonably well when non-adiabatic transitions occur between a small number of PES, but not for a dense manifold of excited states. Perhaps the most sophisticated way to go beyond Ehrenfest in a controlled manner is the *Correlated Electron-Ion Dynamics approach* (CEID) [85]. CEID relies on expansions of the von Neumann equation for the electron-nuclear system, with different formulations proposed in the limits of weak and strong electron-nuclear coupling. Although CEID is still rather young and costly, it has emerged as a powerful tool for problems in which the transfer of energy between electrons and nuclei is crucial. A cost-effective alternative that limits the nuclear motion to harmonic phonons, named *Effective CEID*, has been proposed recently [81], and applied to inelastic electron transport in water chains [89]. It is important to remark that none of these methods is presently mature enough to allow for the dynamical simulation of the dissociative electron attachment process. However, it is envisaged that this will become possible in the near future.

3. Dynamics ensuing DEA: from the gas to the condensed phase

In the absence of an adequate methodology for describing the dynamics of DEA and the subsequent evolution, we have resorted to the following approach: we assume that the DEA process occurs over a short time scale and that once this process is concluded the excess electron is trapped in a bound state of a stable anion. In other words, after DEA the DNA and ion form a ground state anion. We assume that the excess electronic energy is transferred into a specific vibrational mode and as such we introduce an instantaneous kick in the kinetic energy by modifying the velocities of the atoms involved in that vibrational normal mode. We then follow the dynamics of the evolution that ensue using BOMD, i.e. a combination of DFT for ground state electrons with molecular dynamics for the nuclei. In the results presented below, we calculated the electronic structure using the ab initio quantum module Quickstep (QS) of the open source computer code CP2K [90]. The Kohn-Sham orbitals and electronic density were represented using the Gaussian and plane waves method (GPW). For the exchange-correlation functional we used PBE supplemented with a van der Waals dispersion correction. GTH pseudopotentials were used in conjunction with the TZVP-GTH basis set. The motion of the atomic system was followed using MD, with a timestep of 0.5 fs. In our simulations, the specific vibrational modes that were excited in the way described above, corresponded to vibration of the N-H bond in the nucleobase and vibration of the C-O bond in the nucleotide.

To increase the vibrational energy of a molecular bond, we modified instantaneously the velocities, and hence the kinetic energies, of the constituent atoms. For an A-B bond,

the new velocities of atoms A and B are given by:

$$\mathbf{v}_A = \mathbf{v}_A^{(0)} + \eta_A \hat{\mu} \qquad ; \qquad \mathbf{v}_B = \mathbf{v}_B^{(0)} + \eta_B \hat{\mu} \tag{7}$$

where $\mathbf{v}_A$ and $\mathbf{v}_B$ are the new velocities and $\mathbf{v}_A^{(0)}$ and $\mathbf{v}_B^{(0)}$ are the unmodified velocity vectors of atoms A and B, respectively. $\hat{\mu}$ is the director of the bond connecting atom A to atom B, which is calculated using:

$$\hat{\mu} = \frac{\mathbf{r}_A - \mathbf{r}_B}{|\mathbf{r}_A - \mathbf{r}_B|} \tag{8}$$

where $\mathbf{r}_{A,B}$ are the position vectors of atoms A and B before the kick. The quantity $\eta_{A,B}$ is the extra velocity that will be added to each atom. This quantity is calculated by identifying the change in kinetic energy with the electronic energy lost by decaying from the resonant state to the LUMO (ΔE)

$$\frac{1}{2} m_A \eta_A^2 + \frac{1}{2} m_B \eta_B^2 + m_A \eta_A \mathbf{v}_A^{(0)} \cdot \hat{\mu} + m_B \eta_B \mathbf{v}_B^{(0)} \cdot \hat{\mu} = \Delta E \quad , \tag{9}$$

together with conservation of momentum:

$$m_A \eta_A + m_B \eta_B = 0 \quad . \tag{10}$$

In these expressions m_A and m_B are the masses of atoms A and B respectively. Combining (9) and (10) we obtain the following quadratic equation for η_A:

$$\frac{1}{2} m_A \left(1 + \frac{m_A}{m_B}\right) \eta_A^2 + m_A \left[\left(\mathbf{v}_A^{(0)} - \mathbf{v}_B^{(0)}\right) \cdot \hat{\mu}\right] \eta_A = \Delta E \quad , \tag{11}$$

with $\eta_B = -m_A \eta_A / m_B$. Typical values of ΔE are much larger than thermal energies, so in principle once could disregard the last term in (11), and hence the new velocities will simply be,

$$\eta_A = \sqrt{\frac{2\Delta E}{m_A(1 + m_A/m_B)}} \qquad ; \qquad \eta_B = -\sqrt{\frac{2\Delta E}{m_B(1 + m_B/m_A)}} \quad . \tag{12}$$

3.1. Nucleobase

We now present results for the dynamics following DEA in a nucleobase. In this study we examined Thymine, in the gas phase, in a microsolvated environment, and finally in the condensed phase. A vibrational analysis showed that the normal mode vibrating with the highest frequency was the N-H bond highlighted in Figure 12 (circled in red). We thus proceeded to investigate the effect of injecting energy into the N-H bond shown in Figure 12 in the manner described ave, i.e. by augmenting the velocity of the H-atom and, to conserve momentum, also augmenting that of the N-atom. This was done after a period of equilibration at room temperature. Simultaneously with the kick, we added an electron to the system, which went on to occupy the LUMO of the neutral system, and turned it into the so-called singly-occupied molecular orbital, or SOMO, of the anion.

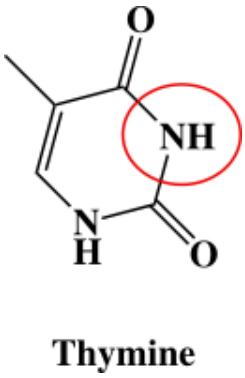

Figure 12. Thymine Nucleobase. The N-H bond that receives the excess energy from the excited electron is circled in red.

3.1.1. Gas Phase. In the gas-phase we expected the bond to break when the N-H bond received an additional energy larger than the dissociation energy, which in this case equals 1.67 eV when it is calculated at the same theory level and using the same basis set as was used for the dynamical simulation. This value corresponds to the dissociation of Thymine into $[\text{Thy-H}]^-$ + H, with H leaving as a neutral species. The calculated dissociation energy for the reaction [Thy-H] + H^- is 5.87 eV, so we do not expect to see the hydride ion at low energies. These dissociation energies are consistent with experimental data [46, 47, 48, 49, 51] which shows that hydrogen atoms are released when Thymine interacts with electrons with energies less than 3 eV, and with results of Ptasinska *et al* [50], who showed that hydride anions are released when Thymine interacts with electrons with energies between 5 and 13 eV. We ran dynamical simulations injecting kinetic energies of 1 eV and 2 eV into the N-H bond. In the first case we observed that the H atom made a large excursion but then returned reforming the bond and redistributing the excess energy amongst the other vibrational modes. For the 2 eV injection, the bond broke and never reformed. We also observed dissociation of the bond in a simulation in which 1.7 eV of additional kinetic energy was added, which is just above the dissociation threshold in the gas phase.

Dissociation energy calculations are possible in the gas phase but not in the condensed phase. In the condensed phase the dissociation fragments are difficult to define because the dissociated system could assume a wide variety of different configurations. In the condensed phase, we would need to calculate the free energy for dissociation, which requires a large amount of statistics to justify convergence. We thus proceeded in a more empirical way and studied different excess energies and analysed whether or not the N-H bond dissociated. The effect of a water environment on DEA was investigated in two steps. We first looked at microsolvation of Thymine by five water molecules, and then we examined the Thymine-water system in the condensed phase.

3.1.2. Microsolvation. The microsolvated system consists of a Thymine base surrounded by five explicit water molecules (See Figure 13). These water molecules make hydrogen bonds with the Thymine at all possible positions involving N and O-atoms (C-atoms do not make significant hydrogen bonds), and were taken from previous studies [63, 91]. The water molecules in this system provide a representation for the first solvation shell of Thymine.

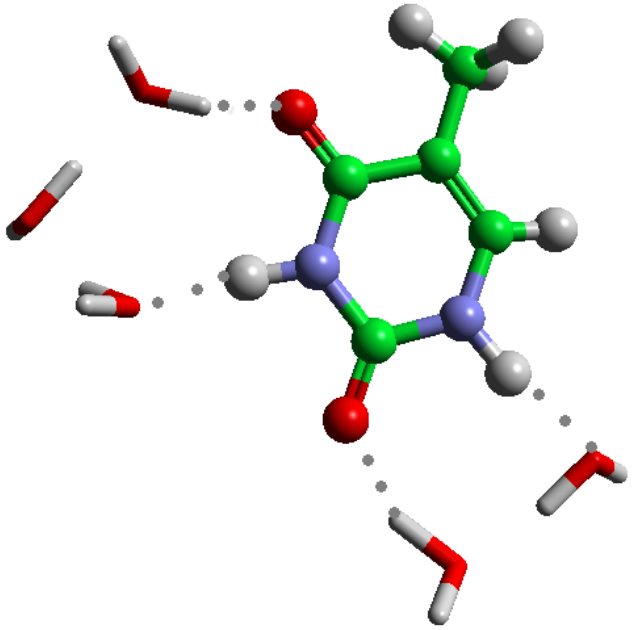

Figure 13. Thymine microsolvated by five water molecules. Two types of hydrogen bonds between water and Thy are present: O–H···O, with water donating the proton, and O···H–N, with water accepting the proton. Dots indicate hydrogen bonds.

In order to estimate the minimum energy required to break the same N-H bond as in the gas phase, we used the method above to calculate new velocities for the N and H atoms, with initial positions and velocities taken from a previous equilibration run. In contrast to the gas phase results, an excess energy of 2 eV was not sufficient to break the bond under microsolvated conditions. The H atom temporarily detached from the nucleobase and interacted with nearby water molecules, but eventually the bond reformed and the excess energy was redistributed among the H-bonded water molecule and the base. When an excess energy of 3 eV was introduced, the H atom had enough energy to reach and collide with a nearby water molecule. In this case we observed a concerted proton transfer process at play. The "kicked" H-atom was transferred as a proton to the H-bonded water molecule, while one of water H-atoms proceeded to leave the system as a neutral atom. The net result was a dehydrogenated Thymine anion $[\text{Thy-H}]^-$, five intact water molecules, and a reversal in the direction of the H-bond from N–H···O to N···H–O. This sequence of events is shown in Figure 14.

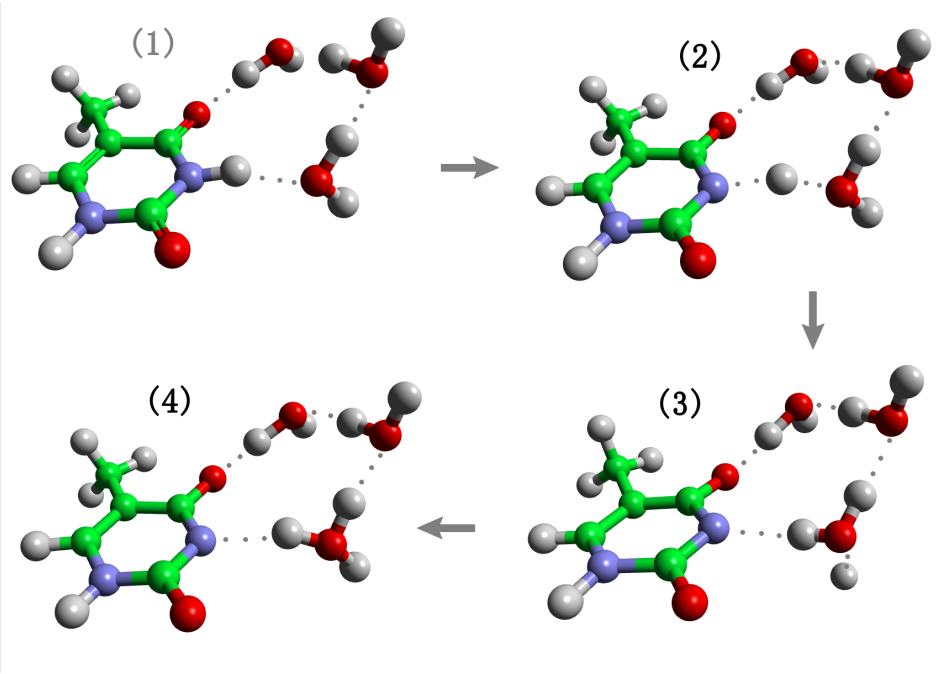

Figure 14. The sequence of events when the H-atom interacts with the water molecule to cause its dissociation. Snapshots are ordered clockwise and numbered, starting from the upper left corner, and the sequence indicated with arrows. Dotted lines indicate hydrogen bonds.

This result implies that dissociation, even in a small amount of water, requires more energy than in gas phase. It would, therefore, seem that some of the energy in excess of the 1.67 eV required for bond cleavage is used in other processes in the microsolvated environment. It is thus tempting to conclude that the energy required to dissociate the bond increases as the number of solvation waters increases. Interestingly, recent experiments in microhydrated Uracil and Thymine support the notion that caging stabilises the anions and supresses fragmentation [92].

3.1.3. Condensed Phase. In this work condensed phase systems have been modelled using periodic boundary conditions in all directions. This allows us to model fully-solvated molecules using a relatively small number of atoms and to remove surface effects. The results obtained in this way are the most comparable with what might occur in cell-like conditions, although the concentration of nucleobase may be somewhat larger than the typical concentrations in cells because of the high ratio between the number of solute and solvent molecules. Our condensed phase model consisted of a single Thymine molecule in a bath of 30 water molecules.

During the equilibration run, the system fluctuated from a H-bonded configuration in which the distance between the H of the N-H group and the oxgyen of the nearest molecule was between 1.5–2.6 Å [93], and configurations in which this hydrogen bond was not present. An example of a H-bonded configuration, with the closest water

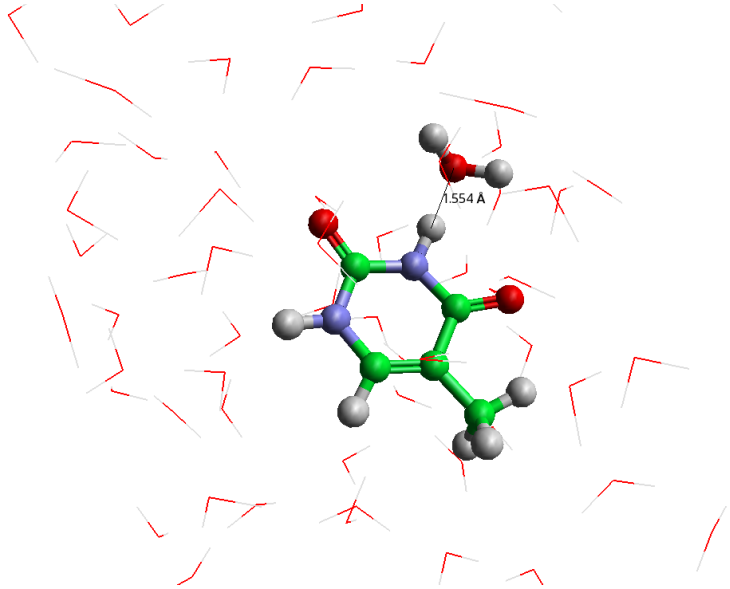

Figure 15. A snapshot from a trajectory for the condensed phase system in which the H-bond is present. In this frame, the H-bond length is 1.554 Å.

molecule and the nucleobase are highlighted, is shown in Figure 15. Typically, multiple fluctuations between H-bonded and non-H-bonded situations are seen multiple times in only 5 ps of simulation. On top of this the we observed that the identification of the water molecule that was closest to the Thymine changed along the simulation.

The microsolvation results suggest that H-bonding between the water and the nucleobase should stabilise the anion and thus increase the energy required to drive the dissociation of the N-H bond. This is consistent with evidence from Kumar *et al* that dissociation barriers are higher when a hydrogen-bond network exists between DNA and the surrounding water environment [94, 95]. On top of this we will show in Section 4.1 of this article that hydrogen bonds between all of the DNA nucleotides and their aqueous environments increase the free energy barriers for bond breaking. To examine what happens to the barrier to dissociation in a fully solvated environment we simulated the post-DEA dynamics in both H-bonded and non-H-bonded configurations of the condensed phase system. To estimate the dissociation energy for the thymine anion in the condensed phase, we chose 15 H-bonded configurations and eight non-H-bonded configurations. We prepared the initial velocities of the N and H atoms for each of these configurations using the method explained above. We first studied their behaviour when an excess energy of 1 eV was introduced and gradually increased this energy, only stopping once the nucleobase dissociated during the subsequent simulation. The energy at which we stopped was a first estimate of the dissociation energy. We also tested energies above our first estimate in order to ensure that dissociation still occurs. Of the 15 H-bonded configurations we examined, we found that 12 required an energy greater than 3 eV to dissociate. Of these, six configurations required more than 5 eV to dissociate, but all configurations dissociated with an energy of less than 10 eV. From

the eight non-H-bonded configurations, seven of these dissociated with an energy of 3 eV or less. The remaining configuration required an energy between 3 and 5 eV.

We focused on the simulations in which 3 eV of excess energy was introduced. We observe two different scenarios in these simulations. When the nucleobase is H-bonded the N-H bond does not break and the excess energy is transferred to the environment. When the nucleobase is not H-bonded, the bond breaks with ease and the hydrogen leaves together with the excess electron in the form of a neutral H-atom, which interacts very weakly with the water environment and hence diffuses away rapidly. The obvious question is, why would dissociation require more energy if there is a hydrogen bond present? A possibility is that energy is more efficiently channelled through the hydrogen bond and delivered to other parts of the system. To investigate this, we calculated the kinetic energy of the N-H bond, the kinetic energy of the remaining atoms in the nucleobase and the kinetic energy of the water molecule that was closest to the hydrogen of the N-H bond, separately. For each of these groups of atoms, we then evaluated the difference between the kinetic energy before and after the "kick". This quantity provides a measure of how much the kinetic energy deviates from its unperturbed, equilibrium value.

Figure 16 shows the running average for the N-H bond kinetic energy as a function of time. The black line is for an H-bonded initial configuration, while the red line is the result in the non-H-bonded case. The blue line is a reference that was obtained by simulating the dynamics without the addition of any kinetic energy. It is clear that the presence of the hydrogen bond influences the system's return to equilibrium as the kinetic energy of the N-H bond decays much more slowly when the hydrogen bond is present than when it is not. When the hydrogen bond is absent (red line), the N-H bond breaks early in the simulation. A significant fraction of the excess kinetic energy is converted into the potential energy required to break the bond, while the remainder is redistributed. When the hydrogen bond was present the trajectories showed that the initial 3 eV of excess vibrational energy caused the H atom to detach but that it rapidly reattached to the nitrogen. The fact that the kinetic energy of the bond decays more slowly in this second, H-bonded scenario, is consistent with the observations. The kinetic energy of the bond does eventually relax down and evolve towards equipartition but the question of where the excess energy goes still remains.

In the H-bonded case, we observed that most of the excess energy is redistributed amongst the vibrational modes of the nucleobase, although a fraction of this energy takes brief excursions to the nearest water molecule. Hydrogen bonds are less efficient than covalent bonds in redistributing vibrational energy, but over a longer time scale the whole system should approach thermal equilibrium. However, environmental fluctuations and anharmonicity prevent the excess energy from returning in whole to the N-H bond and thus frustrate the breaking of this bond. In the non-hydrogen bonded case, the kinetic energy of the nearest water molecule fluctuates in a similar way to the equilibrated system but there are no indications of a transfer of energy away from the N-H bond.

We can, therefore, conclude that the hydrogen bond serves both as a channel to

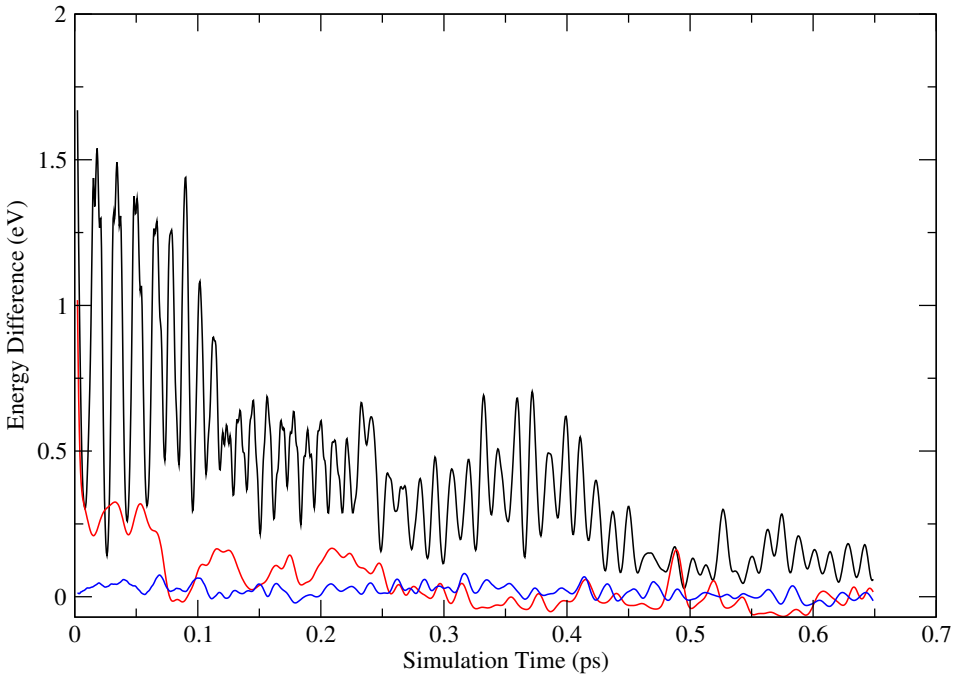

Figure 16. The change in kinetic energy of the N-H bond. The black (red) line corresponds to a H-bonded (non-H-bonded) initial configuration. The blue line shows the change in the kinetic energy in simulations when no additional kinetic energy was injected into the N-H bond.

transfer energy to the surrounding solution and as an obstacle that reflects energy back into the nucleobase. The hydrogen bond has a *caging* effect on the dynamics of the hydrogen atom that forms part of the N-H bond. This process of caging channels the kinetic energy out of this bond and into the surroundings and is thus what prevents it from breaking. The presence or absence of this hydrogen bond is thus crucial for understanding whether or not the nucleobase will dissociate via DEA in solution. It is known that the thymine anion is a weak base, with a pK_a=6.9 [96], which suggests that there will be similar fractions of H-bonded and non-H-bonded base anions. A more precise determination of the propensity for this hydrogen bond to form requires the use of molecular simulation techniques (work in progress).

3.2. Nucleotide

The previous section gives an insight into the effect of solvation on post-DEA dynamics, and shows that nucleobases such as Thymine are more stable against DEA when they are in solution than they are in gas phase because of hydrogen bonding and caging effects. This, however, is not directly relevant to DNA strand breaks as any base in DNA is attached to a sugar and a phosphate, and H-boned to another base. The next step, then, is to move to the simplest model that contains a C-O bond like those in a phosphodiester bond. Deoxythymidine monophosphate (dTMP) is a nucleotide

composed of a Thymidine nucleoside and a 5' phosphate component. Several studies have shown that, instead of breaking at the 5' C-O bond, strand breaks are significantly more likely to occur at a 3' bond. Therefore, instead of studying the standard dTMP, we have focused on the variant containing a 3' bond that is shown in figure 17. We are interested in the dissociation energies and dissociation products associated with breaking the 3' bond and in any differences that occur when the nucleotide is in different environments. We can estimate the energy required to break the C-O bond in the gas phase and then compare this energy to that required when an aqueous environment is introduced.

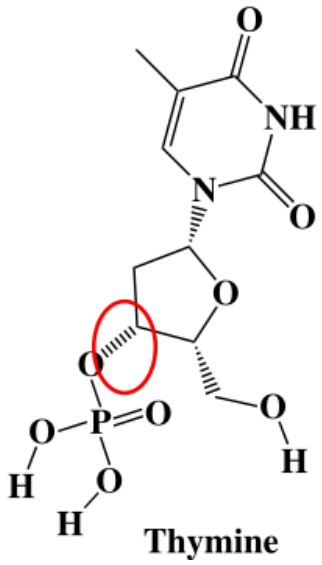

Figure 17. The Thymine nucleotide that was studied in this work with the 3' C-O bond within it highlighted.

3.2.1. Gas Phase. We expect the C-O bond to break when the kinetic energy injected into this bond exceeds the dissociation energy as it was seen for the nucleobase. The nucleotide anion can break by either releasing a Thymidine anion ($dThd^-$) and a phosphoric acid radical (H_2O_4P), or by releasing a Thymidine radical (dThd) and a stable phosphoric acid anion ($H_2O_4P^-$). Calculations performed at the PBE/TZVP-MOLOPT level indicate that the first of these two reactions requires an energy of 1.23 eV, while the second one only requires 0.08 eV. Therefore, the most likely dissociation products of $dTMP^-$ are the neutral nucleoside and a negatively charged phosphoric acid. This is in agreement with a number of experimental studies, which have also found that DNA damage can occur at these low energies because of charge transfer. It is interesting to note that the initial experiments of Sanche *et al* did not observe damage in plasmid DNA by electrons with energies as low as these [1]. However, later experiments by the same group found DNA strand breaks were possible at energies

between 0 and 4 eV, with damage peaks at 0.8 ± 0.3 eV and at 2.2 eV [42]. Simons [73] proposed an explanation for this very low energy strand break in DNA in terms of a vibronic coupling between the π^* orbital of the nucleobase and the σ^* orbital located in the C-O bond. This coupling allows the electron to transfer its energy to the C-O bond and cause bond cleavage.

A vibrational analysis of dTMP identified the C-O bond as a clean normal mode, with very little weight in other parts of the molecule. Therefore, the additional energy was introduced by modifying the velocities of the C and O atoms using the method described above, while adding the extra electron to the LUMO. In the dynamical simulations we observed that dTMP will dissociate when only 0.7 eV of additional kinetic energy is injected into the C-O bond. In the simulation the excess electron is seen to transfer from the nucleobase to the C-O bond to facilitate its cleavage. The evolution of Mulliken charges shows that, after cleavage, the excess electrons stays with the phosphate, forming a phosphoric acid anion, which is consistent with the picture presented by the dissociation energies presented above. Dissociation also happens at all higher energies.

3.2.2. Microsolvation. The microsolvated system consists of a dTMP molecule and the 19 surrounding water molecules that complete its first solvation shell [97]. An excess electron was added, and simultaneously an excess kinetic energy of 1 eV was given to the C-O bonds of three equilibrated configurations of this system. In all three cases, the bond extended, but quickly reformed, showing that this is not enough energy to cause dissociation. Simulations with 2 eV broke the bonds in some cases, while 3 eV led to dissociation in all cases. We therefore conclude that in a micro-solvated environment the energy required to dissociate the bond is much higher than the dissociation energy in gas phase, and it may increase further in the fully solvated environment.

3.2.3. Condensed Phase. The condensed phase model consists of a single dTMP molecule and 64 surrounding water molecules in a periodic simulation cell. In the gas phase, dTMP includes a phosphate component with the two O-H bonds (O_i-H and O_j-H) that are circled in red in Figure 18, i.e. it is *doubly protonated*. During condensed phase equilibration the neutral nucleotide proved itself to be prone to deprotonation at the O_i-H or O_j-H sites. The molecule therefore probed *singly protonated* configurations. To investigate the protonation state of the phosphate, we calculated the shortest distances between the two oxygens on the phosphate and all the hydrogens in the system to which they could form bonds, including all the hydrogen atoms in the water molecules. Figure 19 shows these distances as a function of time. Covalent O-H bonds should be approximately 1 Å in length, so it is clear from this figure that the phosphate is more often singly protonated than doubly protonated.

Dynamical simulations were run on both types of configuration, singly and doubly protonated, following the procedure described above. These simulations were started from configurations taken from the equilibration. Doubly protonated configurations

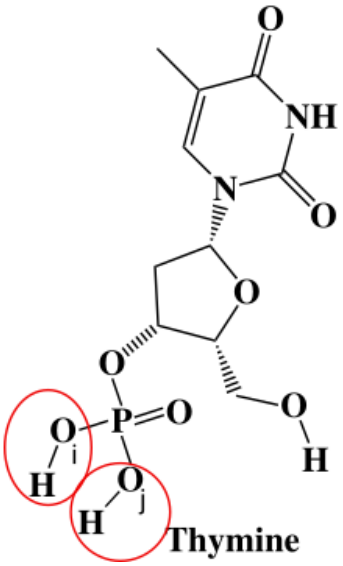

Figure 18. Thymine Nucleotide: the two O-H bonds on the phosphate component are circled in red.

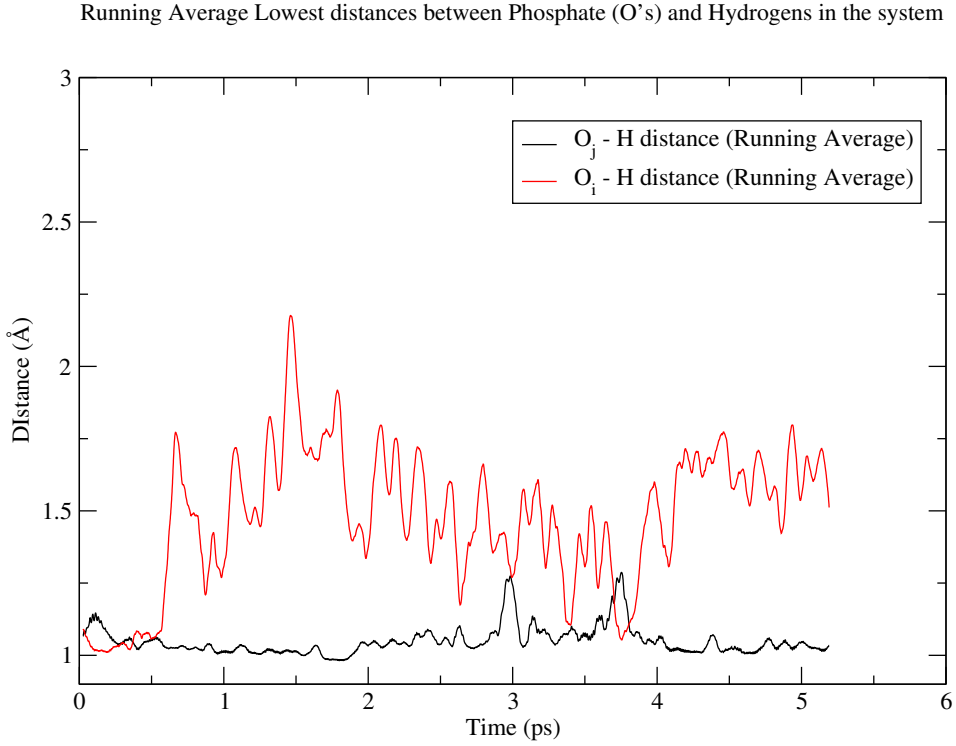

Figure 19. Running averages for the shortest distances between phosphate oxygens and the hydrogens atoms in the system. O-H covalent bonds should be approximately 1 Å in length, so this figure suggests that the phosphate group is more likely to be singly protonated.

dissociated when an excess kinetic energy of 1 eV was introduced to the C-O bond. Most of the singly protonated configurations required at least 2 eV to dissociate. In the singly protonated configurations that dissociated with 1 eV, the phosphates quickly re-gained a second proton when the energy was introduced. This protonation from the water following dissociation seemed to prevent the C-O bond from reforming. Looking at the spin density, we observed that in the doubly protonated case at 1 eV the excess electron transfers to the C-O bond, which breaks. In the singly protonated system, by contrast, the electron remains on the nucleobase and the bond does not break.

It is well known that in aqueous solution nucleotides (and more generally DNA) are prone to deprotonation at the phosphate site [98]. To make further progress the following questions must be investigated: (1) Will the phosphate component of the nucleotide be singly or doubly protonated in condensed phase? (2) Is the dissociation energy of the singly protonated nucleotide higher than that of the doubly protonated nucleotide?

To answer the first of these question we considered the protonation state of the phosphate component from a chemical point of view. The phosphate component of DNA is based on the inorganic acid H_3PO_4 (phosphoric acid), which can undergo the three deprotation reactions shown below:

$$\begin{aligned} H_3PO_4 &\rightleftharpoons H^+ + H_2PO_4^- \quad ; \qquad pK_a = 2.12 \\ H_2PO_4^- &\rightleftharpoons H^+ + HPO_4^{2-} \quad ; \qquad pK_a = 7.21 \\ HPO_4^{2-} &\rightleftharpoons H^+ + PO_4^{3-} \quad ; \qquad pK_a = 12.67 \end{aligned} \tag{13}$$

In the nucleotide, one of the three protons of phosphoric acid is replaced by a carbon atom which joins the phosphate to the rest of the nucleotide. The pK_a value for the second of the reactions above suggests that release of a second proton from the doubly protonated nucleotide is also likely. The release of the third proton is much less likely so the fact that we observe the nucleotide in a single protonated form seems reasonable.

To answer the second question about whether the energy of the single protonated nucleotide is higher than that of the doubly protonated nucleotide we calculated the dissociation energy of the singly protonated nucleotide for the following gas phase reaction

$$dTMP^- \rightarrow dThd + HPO_4^- \tag{14}$$

and obtained values of 3.47 and 3.41 eV for the O_i-H O_j-H sites, respectively. These numbers are significantly larger than the dissociation energy for doubly protonated dTMP which was 0.08 eV. Thefore, if the nucleotide is in a singly protonated state, it is unlikely to dissociate with energies below 3 eV, which is consistent with the results from the dynamical simulations that were presented above.

The literature presents some ambiguity associated with the DEA reaction in solvated DNA. It is generally believed that electron attachment to DNA bases is highly likely when DNA is in solution as there is a large amount of evidence to support this [98, 91, 99, 100, 101, 102, 103, 104]. However, contrasting results suggest that DNA

damage is less likely to occur in solution, as dissociation barriers for the C-O bonds are higher in solution than in gas phase DNA [72, 105, 106, 107, 108]. The results presented here, which show that deprotonation of the phosphate disfavours the C-O bond cleavage, provide an explanation for this ambiguity and give further support for the conclusion that nucleotide dissociation is less likely in condensed phase than in gas phase.

3.3. Larger DNA models: polynucleotides and double strands

At high electron energies, resonances are likely to lead to bond breaks and the cleavage of the 3' phosphodiester bond in particular. In DNA, however, nucleotides are part of the double helix scaffold. This ensures that they are bonded to other nucleotides through 5' phosphodiester bonds as shown in Figure 3 and that the bases are linked to the bases of the complementary nucleotide in the other strand, via hydrogen bonds. The consequence of all this is that DNA has quite a rigid structure. Furthermore, because any phosphate excised via the cleavage of the 3' bond remains attached to its successive nucleotide via a 5' bond, it will not have an opportunity to move too far away from the cleaved sugar component. There is, thus, a distinct possibility that the cleaved 3' bond will be re-formed after only a short period of time. A view of a solvated fragment of DNA made of 12 base pairs is shown in Figure 20.

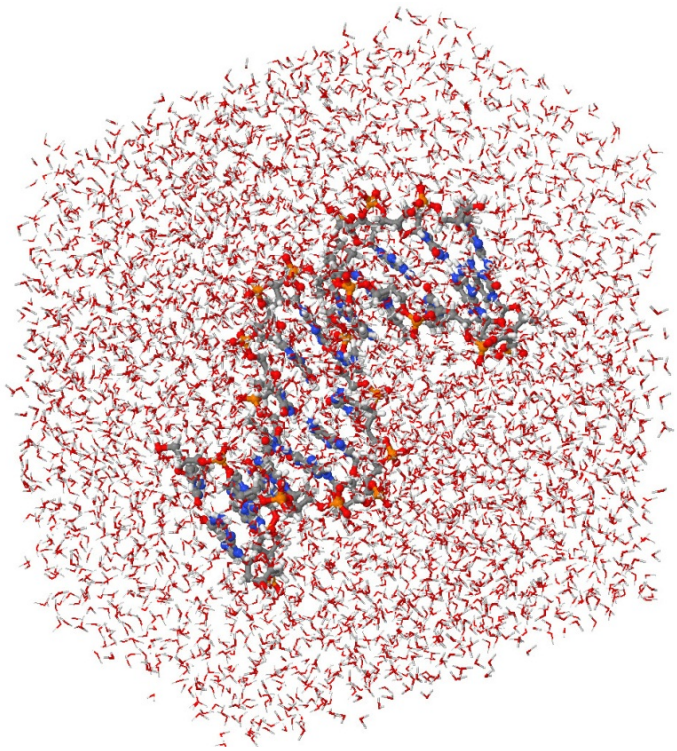

Figure 20. A fragment of DNA composed of 12 base pairs, and solvated in water. This is the smallest stable fragment, and comprises two turns of the helix.

What keeps single-stranded polynucleotides in tact are the (non-bonded) stacking interactions between the bases. These are weak van der Waals forces, but they may still be sufficient to maintain the the structure of the polynucleotide even in the presence of a strand break. These interactions may therefore favour the reforming of the bond. Obviously, these interactions will not help single-stranded DNA to repair itself. Single stranded DNA forms occur during replication, when the H-bonded network between the two strands is unzipped by the action of a combination of enzymes, and a second strand is synthesised by DNA polymerase. It may therefore be more difficult to repair strand breaks if they occur during the replication phase, which will happen more often in frequently dividing cells.

In single-stranded DNA (or RNA) fragments, a particularly interesting question is whether there are specific nucleobase sequences that favour the cleavage of the glycosidic and phosphodiester bonds. This matter was addressed experimentally by Li *et al* [109] in TXT trinucleotides, where T is thymine and X is any of the four bases. Both types of bonds were observed to cleave, and trends were identified according to the identity of the central base X. Simons' argument of a two step process for electronic transfer and bond breakage [73] can be extended to the case of polynucleotides. Excess electrons attach at the base, and when a phosphodiester bond stretches it transfers and cleaves the bond. For a trinucleotide there are four possible such bonds that can cleave, apart from the glycosidic ones. These are shown schematically in the left panel of Figure 21. The other two panels illustrate the previous concept. Before cleavage the excess electron, whose probability distribution is represented here by a blue surface, is located at one of the end bases, in this case thymine (middle panel). When the C-O bond is stretched, the excess electron transfers to the phosphate involved in this bond (right panel) [110].

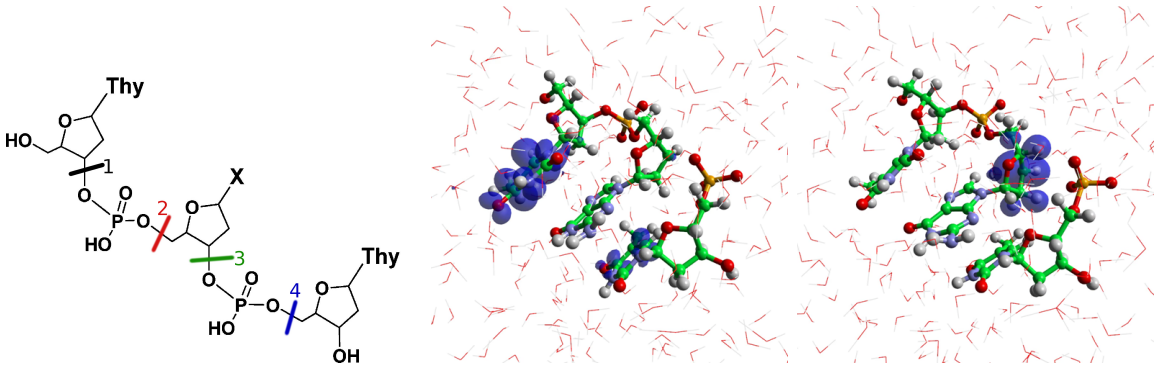

Figure 21. TGT trinucleotide. Left panel: schematic representation showing the four possible phosphodiester bonds that can be cleaved (numbered 1 to 4). Middle and right panels show the location of the excess electron (blue surface) before and after the cleavage, respectively.

Related experimental work was carried out earlier for GCAT tetranucleotides in which G or A had been removed [111]. In this work it was shown that the capture probability depends on the sequence, while bond cleavage is not significantly affected by

the base deletion [112]. Experimentally it is very difficult to disentangle electron capture from bond cleavage at the level of cross sections, as gel electrophoresis distinguishes only the final products. From the theoretical point of view, under DEA conditions the electronic and vibrational states are correlated, and so are the capture and cleavage cross sections. If, however, caging effects due to the environment prevent the direct cleavage, then capture and bond cleavage become independent events. This will be discussed in next Section.

In double-stranded DNA the question arises of where is the excess electron going to localize in a base pair. This is relevant for the capture cross section. Gas-phase calculations indicate that the pyrimidines thymine and cytosine are favoured. In the condensed phase, however, environmental fluctuations can modify this behaviour, as shown in Figure 22.

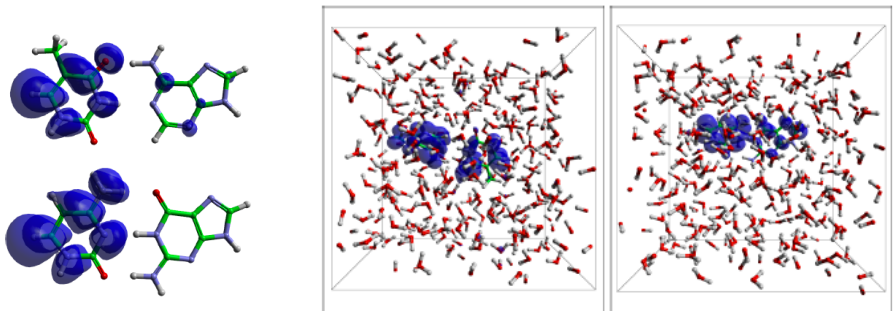

Figure 22. Left panel: AT (top) and GC (bottom) base pairs in the gas phase. The blue surface represents the probability distribution of the excess electron. Right panel: same as left, but in a solvated environment. Delocalization between the two bases can be observed.

The study of DEA in a double-stranded situation requires the identification of which bonds are coupled to the resonant electron, as a function of energy, which is a highly non-trivial matter. Once these bonds have been identified, one could attempt a simulation approach similar to that used for the nucleobase or the nucleotide, above. In such cases, a single strand break will alter the spatial configuration of the helix, twisting it in unnatural ways that can be detected by the enzymatic repair machinery. The question here is whether the phosphodiester bond will reform naturally, or whether there is some aspect in the way it breaks, that prevents it from reforming. If the geometric distortion of the helix is too large, then it is unlikely that the molecule will be able to find the way back to the repaired state. On top of this the strand break may result in chemical modifications to the phosphate and the sugar that raise the free energy barrier to bond reformation. These hypotheses and their likelihood can be assessed using simulations similar to those described in Section 3.2.

4. From DEA to thermal activation

In Ref. [73], Simons described a mechanism to explain how very low energy electrons cause strand breaks in DNA. In Simons mechanism low energy electrons attach to the π^* orbital of the nucleobase and form a shape resonance. They then transfer to a σ^* orbital of the sugar-phosphate C-O bond. This transfer relies on thermal vibrational motion of the neutral molecule and also on the lifetime of the resonance. During the thermal motion, the C-O bond vibrates around its equilibrium bond length of 1.45 Å. If an electron with energy ~ 1 eV is resonantly attached to the molecule when the C-O bond is vibrating but at a length smaller than 1.8 Å, the electron will be captured in a base π^* orbital. If, within the lifetime of the resonance, i.e. before the electron detaches, the C-O bond stretches beyond 1.85 Å, then the σ^* state becomes lower in energy than the π^* orbital, the electron migrates towards the σ^* orbital, and breaks the C-O bond. The C-N glycosidic bond is also susceptible to break, but the barrier is higher.

The likelihood that DNA damage would occur at one of the C-O bonds at such low electron energies was confirmed by experiments performed in Sanche's group. These authors exposed oligonucleotides (CGTA and GCTA) to near-zero eV electrons and discovered that cleavage was primarily along the C-O backbone [113]. These findings led to numerous studies of strand breaking reactions in ground state situations, under conditions where bond cleavage is reliant on thermal vibrational motion. These studies focus on the ground state electronic structure of DNA anions whilst activating the bond stretching. This is generally done by fixing the value of a relevant reaction coordinate, generally a bond length, and computing the energy as a function of the reaction coordinate via constrained optimisation techniques. This allows for the computation of activation barriers and detachment energies at zero temperature, without considering the thermal fluctuations of the environment. Numerous theoretical studies using both wavefunction and DFT methods support the notion that strand breaks can be triggered by such low energy electrons. Bao *et al* [72, 105] calculated the activation energies for bond cleavage in the pyrimidine nucleotides and found that C-O strand breaks should dominate at near-zero energies. By calculating the detachment energies from the base they also showed that it is feasible that electron attachment to the nucleobase can trigger bond cleavage [114]. Barrios *et al* explored the energy surfaces leading to bond cleavage and also found that C-O cleavage would be operational at such low energies [41, 115].

The results in Sections 1.4 and 3 highlight the importance of including the aqueous environment when considering DEA in DNA. The environment stabilizes the resonance increasing its lifetime, thus buying time for energy transfer to occur, which is consistent with the mechanism proposed by Barrios *et al* [41]. In addition, the energy required to break a bond is higher in solution than in gas phase because of caging effects. If the situation is such that the excess energy of the resonant electron is transferred to the C-O bond and if the environment does not allow the bond to break because it reflects vibrational energy back into the nucleotide and dissipates it into the environment, then a thermodynamic equilibrium will be established after a short period. In that

case the system becomes a ground state anion immersed in a fluctuating environment. Under these circumstances, *DNA strand breaks can still occur, but as thermally activated processes*, controlled by a free energy barrier.

The thermal activation mechanism is as follows: as the environment experiences thermal fluctuations at the temperature of interest (room temperature in our case), the bond in question randomly performs excursions away from its equilibrium position. When the bond is stretched, the energy will increase and put it in an unfavourable situation. The Boltzmann factor ensures, however, that if that energy increase is not too high, these fluctuations in bond length carry a non-negligible probability. The larger the stretch, the higher the energy and the lower the probability. Occasionally, the bond can stretch to the point in which the energy reaches its maximum, i.e. the *transition state*. Beyond that point, the bond breaks and the system evolves towards a product state that consists of two fragments. In the present case, one fragment will be negatively charged, and the other will remain neutral. Furthermore, one will be a radical, and the other a closed-shell molecule.

The description of this process is different from that of DEA. We have to start from the attachment of the excess electron to the DNA fragment, i.e. the insertion of an electron into the LUMO of the neutral fragment and the conversion of this orbital into a singly-occupied molecular orbital (or SOMO). A first question is where is the SOMO spatially located, and whether it is similar or different to the LUMO. Secondly, we must ask whether the neutral geometry is suited for binding an additional electron or whether a structural reorganisation is required. Then, we need to identify the bond (or bonds) that are prone to break. That is to say we need to identify the bonds that are weakened by the addition of the electron so that we can study the energy (at zero temperature) or free energy (at finite temperature) profile as a function of the length of these bonds. In this Section we will focus on these questions.

4.1. Electron Affinities

The electron attachment properties of DNA subunits can be investigated through the *electron affinity* (EA). This measurable quantity is the difference between the energy of a neutral molecule and the energy of the anion following electron attachment (TNI).

$$\mathrm{EA} = E_{neutral} - E_{anion} \tag{15}$$

The more positive the EA is, the more likely the molecule will be to attach an electron. The anion and the neutral molecule have two different potential energy surfaces. The characteristic attachment energies, i.e. the difference between neutral and anion energies, depend on the experiment performed, but are usually one of the following three quantities:

(i) Vertical Attachment Energy (VAE): the difference in the energies of the anion and the neutral molecule for the optimised geometry of the neutral molecule.

(ii) Vertical Detachment Energy (VDE): the difference in the energies of the anion and the neutral molecule for the optimised geometry of the radical anion.

(iii) Adiabatic Electron Affinity (AEA): the difference between the energy of the optimised anion and the optimized neutral molecule.

Experimentally, the two most commonly used methods to measure AEA are photoelectron spectroscopy (PS) and Rydberg electron transfer (RET) methods [116]. Experimental AEA values provide benchmarks for theoretical approaches. According to PS, the AEA of uracil is 0.15-0.16 eV [117], while the RET value is 0.06 ± 0.03 eV [118]. Positive values suggest that electron attachment is favourable.

Theoretical studies of electron attachment to DNA subunits were pioneered by Colson, Belson, and Sevilla approximately 25 years ago using the Hartree-Fock (HF) approximation [119]. Subsequently, EA values were refined using post-HF methods that introduce electron correlation at different levels, including second order Møller-Plesset perturbation theory – MP2 –, coupled-clusters including perturbative triple excitations – CCSD(T) –, and multiconfigurational perturbation theory – CASPT2. The AEA values of uracil calculated using *ab initio* methods are presented in Table 1 and are compared to the experimental values. It should be pointed out that the theoretical values include a zero-point vibrational correction. It is clear that HF severely underestimates the AEA of uracil. MP2 and CCSD get closer to experimental values with large basis sets. The most accurate molecular orbital approach, however, is CASPT2.

Table 1. Adiabatic Electron Affinity of Uracil: Ab initio.

Theory level	AEA (eV)
HF	-1.00 [119]
MP2	-0.21 [120]
CCSD(T)	-0.05 [120]
CASPT2	0.03 [120]
Experimental Method	**AEA (eV)**
RET	0.06 ± 0.03 [118]
PS	0.15-0.16 [117]

It is important to remember that these methods are very sensitive to the choice and the size of the basis set that is used to represent the molecular orbitals, especially for calculating EA. Anions are frequently loosely bound and require diffuse basis orbitals and large basis sets. In fact, the additional electron is often not bound so its wave function should be a plane wave. If the basis set used in simulations of such systems is composed of local orbitals like Gaussians, it will produce an artificially bound state at a positive energy that will become increasingly closer to zero as the size of the basis set is increased. This is a signature that something is wrong with the calculation. It happens mostly with the VAE, as most molecules struggle to bind an additional electron at the neutral geometry. It is less relevant for the AEA and the VDE, as the anion is already at its optimised geometry, and the neutral molecule is usually stable in its own geometry and in that of the anion.

Whilst advanced wavefunction methods are highly accurate, their application is limited to relatively small system sizes. Density Functional Theory (DFT) is an attractive alternative because of its reliability and affordability. This method allows one to model relatively large molecular systems with a reasonably high accuracy. DFT calculates the ground state energy of a system as a functional of its electronic density while approximating the exchange and correlation (XC) component of the energy functional. The simplest XC approximation is the time-honoured local density approximation (LDA), which produces significant errors when computing AEAs [121]. The next rung in the ladder is the Generalised Gradient Approximation (GGA), that includes the density and its gradient. AEA for DNA and RNA bases have been computed using the BLYP and PBELYP functionals. Values for Uracil are reported in Table 2. The BLYP affinity is fortuitously close to the PS experimental value.

Table 2. Adiabatic Electron Affinity of Uracil: DFT.
(*includes zero-point vibrational energy correction)

Functional	AEA (eV)
GGA	
BLYP	0.15*[122]
PBELYP	-0.18 [123]
Hybrid	
B3LYP	0.24*[122]
M05-2X	0.17 [36]
M06-2X	0.11 [36]
Experimental Reference	
PS	0.15 ± 0.12 [117]

More accurate functionals are constructed by combining GGAs with HF (exact) exchange in an appropriate proportion. This is the case for the hybrid B3LYP functional [124, 125], which has proved itself to be particularly reliable for predicting AEAs of DNA components [122]. A further step up is to combine the hybrid exchange with a meta-GGA that includes not only the gradient of the density, but also the kinetic energy density (laplacian). This formalism is used in the functionals that belong to the Minnesota suite (M05-2X and M06-2X [126, 127]). These have recently been shown to provide the best comparison to the references in electron attachment calculations. AEAs for Uracil computed with the various functionals are reported in Table 2 and are compared against experimental reference data.

4.2. Base specificity

Uracil is the nucleic acid with the smallest number of atoms so it is widely used in preliminary calculations to make comparisons between theoretical methods so that a

suitable method for examining all other nucleobases and larger units can be settled on. Interestingly, there are significant differences in the electron affinities of the four DNA bases which are consistent across all levels of theory. Table 3 summarizes the AEA values that have been obtained for all the bases using the various methods described in Section 4.1. Whilst the actual values of the AEAs of each of the bases differ with each method, the trend in the ordering is consistent. The purine bases (Gua and Ade) have the lowest electron affinities. The extensive theoretical review by Gu *et al* states that "Electron attachment to gas-phase guanine is not viable and that adenine in the gas phase would not be a good electron acceptor." [36]. The electron affinity of cytosine is predicted to be higher and closer to zero. However, whilst having slightly positive predicted AEA values, gas phase cytosine is an unlikely host for the excess electron and as such thymine is the most likely electron host as it has the highest AEA values.

Table 3. Adiabatic Electron Affinities (eV) for the four nucleobases at different levels of theory (all values include the zero-point vibrational contribution).

Ab initio				
Method	Thymine	Cytosine	Adenine	Guanine
MP2 [120]	-0.26	-0.4	-0.71	-1.06
CCSD [120]	-0.09	-0.17	-0.84	-0.44
CASPT2 [120]	0.02	-0.10	-0.44	-0.72
Density Functional Theory				
M05-2X [36]	0.12	-0.05	-0.35	-0.54
M06-2X [36]	0.07	-0.08	-0.36	-0.54
B3LYP [122]	0.20	0.03	-0.28	-0.10
BLYP [122]	0.12	-0.01	-0.19	-0.01
PBE0 [128]	0.133	0.02	-0.024	-0.04
Experiment				
PS	0.15 ± 0.12 [117]	0.10 ± 0.12 [117]	1.51 ± 0.05 [129]	0.95 ± 0.05 [129]

In summary, the pyrimidines, i.e. Uracil, Thymine, and Cytosine, are the bases with the largest electron affinities and are thus the most likely to attach an electron. Guanine and Adenine exhibit negative values and are therefore unlikely to capture an electron. If we put the bases in order of decreasing AEA, we obtain the following sequence: U $\geq$ T $>$ C $>$ A $\sim$ G.

4.3. Solvation effects

The low-energy interaction and dissociation mechanisms which have been described in the previous sections were mostly investigated by performing experiments and

calculations on dry (gas-phase) DNA fragments. However, in a living cell DNA is in a condensed phase environment and is surrounded by other components including water which is the most abundant species in the cell and which plays a vital role in maintaining DNA structure and function [130, 131]. In both theory and experiment, LEE interactions with DNA are modified in the presence of the aqueous environment. During all the stages of a chemical reaction, the solvent interacts with the solute and thus influences the thermodynamics and kinetics of the reaction. In computer simulations, the effect of solvation can be introduced either explicitly or by using a continuum model. Discrete (or explicit) solvation involves direct addition of water molecules to the solute model. Polarizable continuum solvation models (PCM), sometimes also called reaction fields, cut the computational cost of considering each molecule in the solvent explicitly by placing the molecule in a cavity carved in a medium characterised by a dielectric constant. In the simplest PCM, the dipole moment of the molecule, which is placed in a spherical cavity, polarises the medium, which in turn produces an electric field in the cavity and leads to an effective electrostatic interaction between solute and solvent. More sophisticated models that take into account the shape of the molecule and higher moments of the charge distribution[132] are nowadays implemented in most quantum chemistry codes. PCMs proved effective in studying electron attachment to DNA, but they do not include specific interactions such as hydrogen bonds between solute and solvent molecules. H-bonding is known to stabilize the excess electron in the solute, thus increasing the electron affinity [91]. To overcome this issue, PCMs can also be combined with explicit solvation methods by considering a first explicit solvation shell embedded in a polarisable continuum.

4.3.1. Solvation effects on electron attachment. AEA values for DNA bases are known to increase in the aqueous environment so solvated DNA is a better electron host. Gu *et al* [98], employed DFT-B3LYP calculations to investigate the influence the aqueous environment has on electron attachment to single stranded DNA. In his simulations the electron capture ability increased significantly when the solvent effects were included via a PCM. In gas phase, the AEA values of the DNA nucleotides were within the range 0.1-0.35 eV whereas, in aqueous solution, the AEA values increased to 0.95-1.99 eV.

The influence of discrete microsolvation on the electron capture ability of the DNA base thymine has been extensively investigated by Kim *et al* [101], who performed DFT-B3LYP calculations with up to 5 water molecules. They found that AEA values increased gradually with the number of hydration molecules and hence that the hydrated anions were more stable than the gas phase anions. AEA values increased to 0.91 eV with 5 water molecules. Dedikova *et al* also predicted, using post-HF, coupled cluster (CCSD) methods, that the AEA of uracil would increase upon addition of up to three water molecules. They calculated a predicted value of 0.42 eV for the tri-hydrated uracil cluster [103]. The effect of an increased number of water molecules in the solvation shell, up to 15, was computed at the DFT-PBE0 level of theory [91]. In line with Kim *et al* , the AEA of each of the bases increases with the number of molecules and saturates at

values of around 1 eV, as shown in Figure 23.

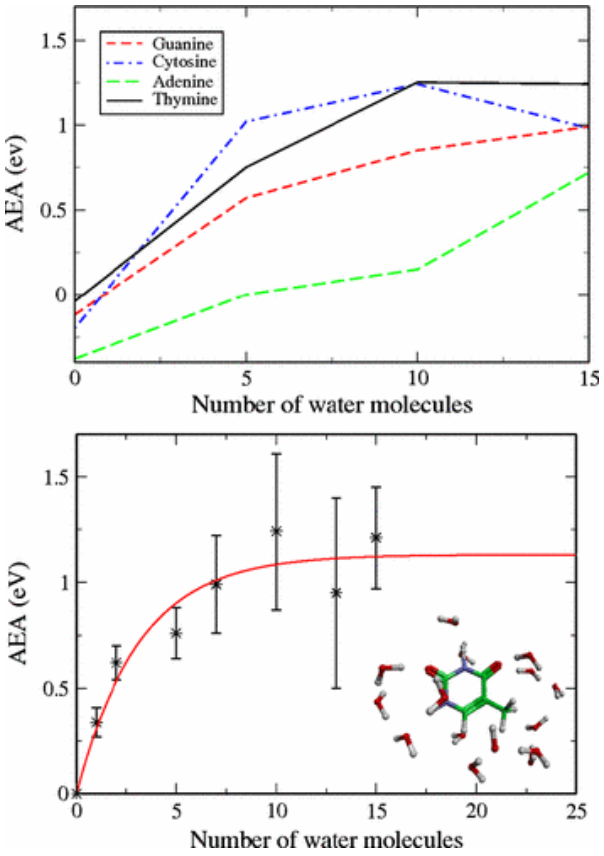

Figure 23. AEA values for each of the nucleobases with an increasing number of surrounding water molecules. Reprinted with permission from M. Smyth and J. Kohanoff, Phys. Rev. Lett. **106** 238108 (2011). Copyright 2011 by the American Physical Society.

Schiedt *et al* [117] investigated electron attachment to micro-solvated uracil, thymine and cytosine using photodetachment-photoelectron (PD-PE) spectroscopy experiments. The electron affinities obtained from the PD-PE spectra showed that the average increase per added water molecule was 0.22 eV for uracil, 0.20 eV for thymine and 0.17 eV for cytosine. These experimental values are consistent with the calculated ones.

4.3.2. Solvation Effects on Dissociation. The electron capture ability of DNA fragments increases as the level of solvation increases but there is ambiguity surrounding the dissociation of these molecules in solution. In some experiments, hydration can be introduced to films of DNA as monolayers. Ptasinska and Sanche [133] performed anion desorption experiments on short DNA single strands covered by three water monolayers. The anion yield, or in other words the dissociation products, were increased by a factor of 1.6 when in this solution. Furthermore, in recent experiments by Alizadeh *et al* [28], the hydration level was varied up to a bulk-like water environment. The amount of

DNA damage increased significantly in bulk-like water because of the increase in the AEAs of DNA bases when in solution. However, ambiguity remains because numerous studies that investigated the influence of a water environment on dissociation barriers suggest that dissociation should be more difficult in solution.

Studies by Gu *et al* [72, 105, 106, 107] at the DFT-B3LYP level of theory investigated solvation effects on the cleavage of the pyrimidine strands (C and T) by using a polarisable continuum to model solvation. These studies demonstrated that the activation barriers for C-O and C-N bond cleavage increase significantly when the molecule is moved from a gas phase to a solvated environment. In other words, the aqueous environment greatly increases the activation energies for strand breaks at the $C_{3'}$-$O_{3'}$, $C_{5'}$-$O_{5'}$, and for base excision at the glycosidic bond. Interestingly, guanine displays a different behaviour to the other nucleobases. Schyman and Laaksonen [134], used DFT-B3LYP to investigate the effects of both the PCM and an explicit water environment on $C_{3'}$-$O_{3'}$ cleavage barriers in guanine-3'-monophosphate (dGMPT). They found that cleavage barriers were lower when in solution compared to those calculated in the gas-phase. Further studies by Gu *et al* of the guanine-3'-5'-monophosphate found activation barriers for the cleavage of $C_{3'}$-$O_{3'}$, $C_{5'}$-$O_{5'}$ and C-N bonds were dramatically decreased upon solvation by a PCM [135].

These findings help explain the experimental observation that guanine might be the *weak link* in DNA. Time-resolved laser spectroscopy (TRLS) was used by Wang *et al* [136] to investigate low-energy electron interactions with solvated nucleotides. They found that electron attachment to all nucleotides would occur within 1 ps. Furthermore, these authors found that both dAMP and dCMP nucleotides formed stable anions after electron attachment. However, 35% of the dTMP anion and 60% of the dGMP anion dissociated. In other experiments, Zheng *et al* investigated strand breaks in short DNA sequences (GCAT), where individual bases were deleted selectively to understand their roles. Again, guanine was highlighted as a particularly sensitive damage site because the extent of damage decreased significantly when G or A were removed [111]. These results will be discussed again later within the context of free energy calculations.

The effect of the direct interaction between water and DNA components was also highlighted in DFT studies by Kumar and Sevilla [94], who modelled the cleavage of 5'-thymine monophosphate with and without explicit water molecules. Their results showed that the cleavage barriers increased significantly upon solvation. Furthermore, there was a suggestion that some of the waters were hydrogen-bonded to the nucleotide in their optimised structures.

4.4. Molecular dynamics simulations and free energies

While static (zero-temperature) calculations are useful to establish the foundations for understanding DNA damage in solution, they do not take thermal and electrostatic fluctuations in the environment into account, which are non-negligible at room temperature. Moreover, activation energies are generally computed along a specific, one-

dimensional reaction coordinate, such as the length of a C-O bond. Molecular Dynamics (MD) simulations provide a way of incorporating the effect of these fluctuations. The water component can be treated at the same theory level of the DNA fragment, or otherwise using a classical force field within a widely used methodology that has been called QM/MM. First-principles MD simulations (FPMD) where water and solute are all treated at the DFT-PBE level, have been used to simulate the dynamics of the excess electron in an explicitly solvated nucleobase system with 64 water molecules [91]. In pure water an excess electron will roughly localise in a cavity with the water hydrogens pointing towards it [137]. However, when a solute is present the electron localises very rapidly on the nucleobase, over a timescale on the order of 15-25 fs. This fast localisation on the nucleobase was also observed for nucleosides and nucleotides [128, 138].

Free energy barriers for the phosphodiester bond in 3' and 5' cytidine monophosphate (dCMP) were computed by Schyman *et al* [108], using a QM/MM model in which the nucleotide was described at the DFT-BLYP level and immersed in a classical (AMBER) water bath containing over 1000 water molecules. The authors of this study computed barriers for phosphodiester bond cleavage on the order of 30 kcal/mol, which are much higher than the gas-phase barriers. Explicit classical water molecules provide a much better representation of the environment than a polarisable continuum, as they include specific interactions such as hydrogen bonding. What they do not generally do, unless reactive force fields such as Morse potentials are used, is allow for water dissociation and proton transfer. In order to overcome these limitations, free-energy barriers were computed in a fully quantum model for each of the four DNA *nucleotides* surrounded by 100 explicit water molecules [138]. In this work, the gas-phase barriers for the cleavage of the $C_{3'}$-$O_{3'}$ bond were compared to those in static solvation and in a thermally fluctuating solvated environment. The static solvation barriers were the highest by a significant margin, whereas gas-phase and thermally fluctuating barriers were comparable. It subsequently emerged that in that paper there were some problems with the statistical analysis so the free energies for the thermally fluctuating systems were underestimated approximately by a factor of two. This was rectified by McAllister *et al* [139], who reported barriers between 15 and 20 kcal/mol for all nucleotides. This suggests that the energy barriers calculated by optimising the geometry for different values of the reaction coordinate (static barriers) can be significantly larger than those calculated dynamically, thus highlighting the importance of bringing environmental fluctuations into the picture [138].

In addition to the free energy barriers, these simulations provided a clear proof that the strand break mechanism proposed by Simons [41, 73] still operates in the condensed phase. Evidence for this assertion is provided in the spin density plots shown in Figure 24. These images clearly demonstrate that the excess electron is captured at the base. Then when the phosphodiester bond elongates to about 1.8 Å, the electron delocalizes over the whole nucleotide. This electronic state is a combination of the two crossing states, that become degenerate at the transition state. For larger elongations, the excess electron re-localizes on the sugar-phosphate region and the free energy starts decreasing

towards the products basin. Upon further elongation, the bond eventually breaks.

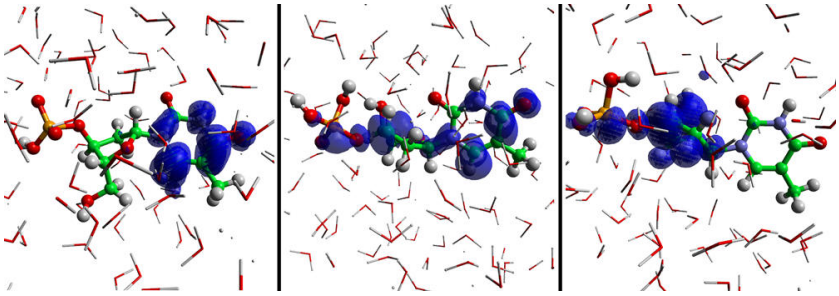

Figure 24. Spin density plots for $dTMPH^-$: (left) at the equilibrium bond length of 1.4 Å; (middle) at the transition state, with a bond length of 1.8 Å; (right) after bond cleavage, at a bond length of 2.2 Å. Reprinted with permission from M. Smyth and J. Kohanoff, J. Am. Chem. Soc. **134**, 9122 (2012). Copyright 2012 American Chemical Society.

4.4.1. Protonation. The authors of Ref. [138] noticed that adenosine monophosphate (dAMPT) behaved differently from the other nucleotides, and required twice as much energy to surmount the cleavage barrier. Upon closer scrutiny, it became clear that the reason for this enhanced barrier height was that the base spontaneously protonated at one of the N sites, by seizing a proton from a nearby water molecule. Notice that these kind of events are not possible if the water molecules are represented by a continuum medium, or with explicit classical force fields that do not allow for dissociation of the O-H bonds. It is not obvious either that this can be observed in a hybrid explicit-quantum/PCM model, as the protonation water may not necessarily be one of those treated explicitly. The explanation given for the increase in the height of the barrier was that the presence of the excess electron on the base attracted the water molecule and thus favoured protonation. Once the base was protonated, this very same proton stabilised the excess electron at the base. Since the cleavage is related to the crossing of two electronic states, one located on the base and another on the sugar-phosphate [73], the stabilisation of the electron in the π^* orbital due to protonation shifts the crossing of π^* and σ^* energies to longer C-O distances - distances on the order of 2 Årather than 1.8 Å. In those additional 0.2 Å, the free energy continues to rise reaching double the value at the transition state (the maximum of the free energy curve). These results are consistent with a study of the protonated cytosine structure by Gu *et al* [98], in which protonation was enforced at the N3 nucleobase site and an analysis of its behaviour in a base pair was performed. This study suggested that protonation stabilised the anion and that, if this was the case, C-O bond cleavage might be less likely than cleavage of other bonds in the system. A consideration of H-bonding and protonation was thus deemed crucial for determining reaction pathways and barriers.

The likelihood for protonation of nucleotides in aqueous solution, and the effect of protonation on free energy barriers, were thoroughly studied for all four nucleotides [139, 140]. This was achieved by means of FPMD simulations in which the lengths

of specific bonds were constrained to a series of increasing values. Thermodynamic integration of the constraint force was then used to obtain the free energy profile (blue moon ensemble). Each nucleotide was placed in a 15 Å periodic box with 100 explicit water molecules, with the electronic structure calculated at the DFT-PBE level.

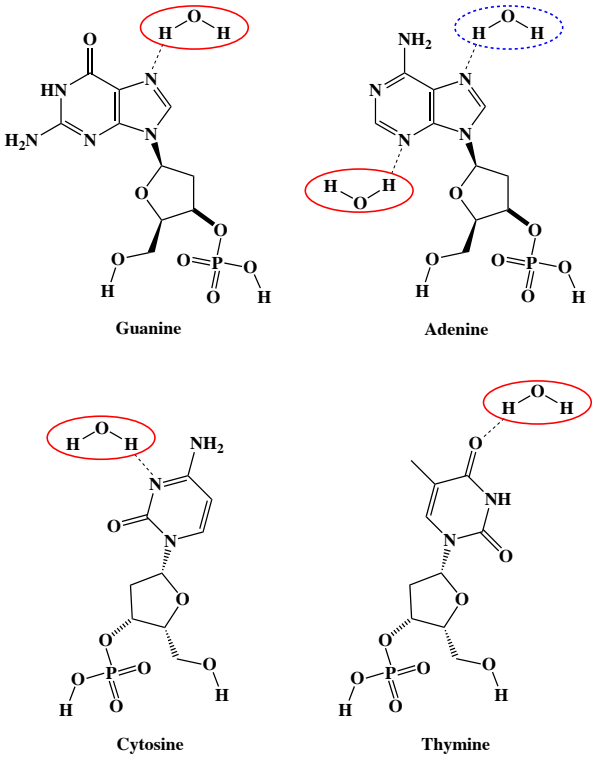

Figure 25. The four nucleotides studied in [139], showing the closest water molecule to each base (circled in red). Protonation was enforced for those hydrogen bonds. In the case of $dAMPH^-$, the water molecule circled in red spontaneously protonated the nucleobase during equilibration and the shortest hydrogen bond was formed by the water molecule dash-circled in blue. Reprinted with permission from M. McAllister et al., J. Phys. Chem. Lett. **6**, 3091 (2015). Copyright 2015 American Chemical Society.

To study protonation a reaction coordinate that measured the shortest distance between an N or O in the nucleobase, and a hydrogen in a water molecule was used. It is important that the hydrogen in this coordinate can belong any water molecule in the system and that a hydrogen belonging to the water molecule that instantaneously is closest to the substrate is not used as the identity of the closest water molecules to the base can change during the simulations [140]. The systems studied are depicted in Figure 25 and the free energy profiles as a function of the distance between the protonation sites and the hydrogen atom belonging to the hydrogen-bonded water molecule are shown in Figure 26.

Figure 26 shows that protonation is favourable for $dCMPH^-$ and $dTMPH^-$, and barrier-less for $dAMPH^-$. This helps to explain why adenine spontaneously protonated

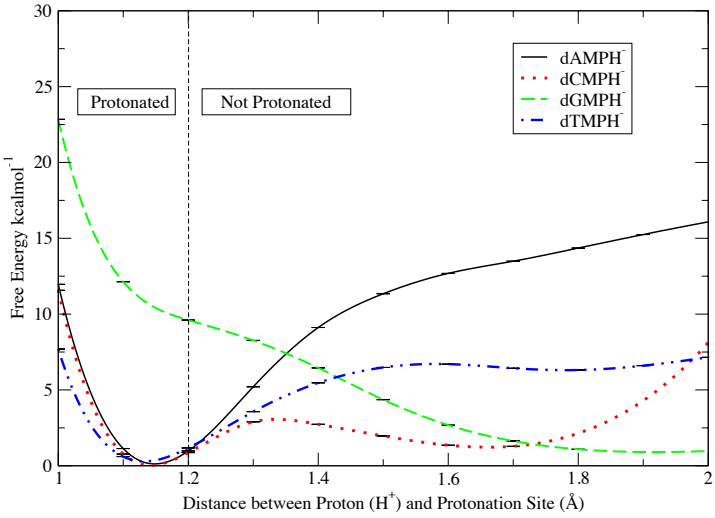

Figure 26. The free energy profiles for the four nucleotides studied in [139]. The vertical dashed line indicates the typical length of a bond involving a hydrogen atom and, thus, indicates the point at which the nucleobase becomes protonated. It is clear that with the exception of $dGMPH^-$, the free energy of the nucleotides is minimized when it is protonated. Reprinted with permission from M. McAllister et al., J. Phys. Chem. Lett. **6**, 3091 (2015). Copyright 2015 American Chemical Society.

during unconstrained equilibration in [138], and confirms that it should be in this protonated configuration when in the condensed phase. There are two minima in the free energy profiles for protonation of cytosine and thymine, one where the nucleobase is protonated and one where the hydrogen atom is covalently bonded to a water molecule and hydrogen bonded to the nucleobase. These minima are separated by a very small barrier, under 1 kcal/mol. Protonation of $dGMPH^-$ is unfavourable, and the minimum in the free energy occurs when the nucleobase is hydrogen-bonded to its closest water molecule. Hence, $dGMPH^-$ will not protonate in the condensed phase.

These calculations suggest that upon electron attachment, in the condensed phase, many of the bases will become protonated. To elucidate the effect of protonation on the strand breaking reactions, free energy profiles were computed by constraining the bond length between the protonation sites and hydrogen atoms used in the protonation calculations (see Figure 25). This was done for two situations, protonated and non-protonated nucleotides. For the protonated nucleotide the bond length was fixed at 1.05 Å, and for the non-protonated case, to 1.8 Å. The non-protonated nucleotide was constrained to ensure that none of the nucleotides would spontaneously protonate during the strand breaks, thus skewing the comparative results. The free energy curves are shown in Figure 27.

Figure 27 shows that the protonation of the base generally makes the strand break reaction more unfavorable. In fact the only exception to this general rule is $dAMPH^-$. For $dCMPH^-$ th effect protonation has is particularly significant. For $dAMPH^-$ - a nucleotide that protonates spontaneously in unbiased MD simulations - the barrier to strand breaking is 4 kcal/mol lower when the system is protonated, but is similar to the

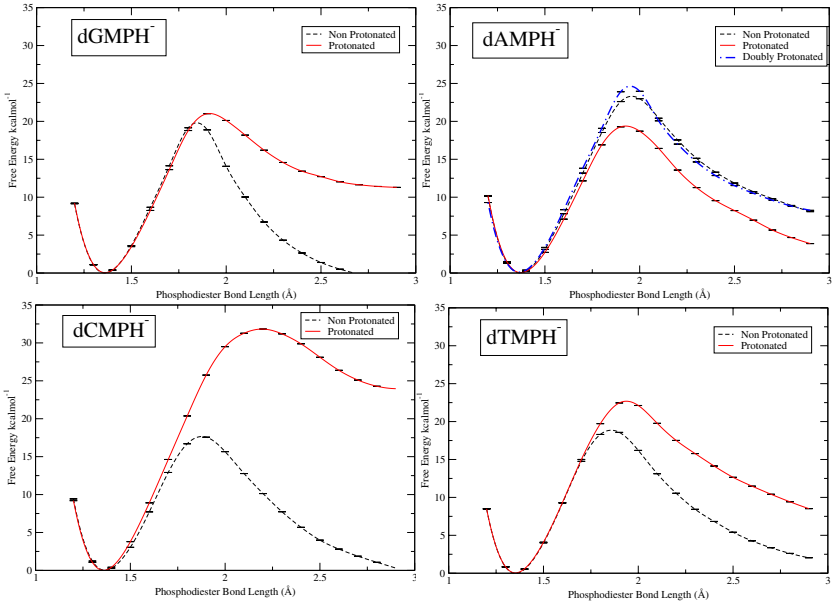

Figure 27. Free energy profiles for the cleavage of the $C_{3'}$-$O_{3'}$ bond in each of the four nucleotide anions. The red lines are for protonated nucleotides and the black dashed lines are for non-protonated nucleotides. It is clear that the protonation state of the nucleotide has an effect on the free energy barrier. In all cases (except for adenine), the barrier to break the bond is higher when the nucleotide is protonated. Reprinted with permission from M. McAllister et al., J. Phys. Chem. Lett. **6**, 3091 (2015). Copyright 2015 American Chemical Society.

barriers for the deprotonated versions of the other bases. This is a consequence of the fact that there is no truly stable hydrogen-bonded configuration for this system. By enforcing a second protonation the strand breaking barrier increases as in the other cases. It is possible to connect these results with experimental observations. For example, Wang *et al* showed that strand breaking is significantly less likely to occur at the Cytosine sites [136] on a DNA strand. This result cannot be explained by examining the free energy barriers for the deprotonated systems as all barriers are similar. However, for protonated $dCMPH^-$ the barrier to strand breaks is significantly higher than for the other bases. This, together with the observation that it is easy to protonate this base (see Figure 26) and the experimental result that the cytosine radical anion is extremely basic (pK_a=13) [141], explains Wang's results.

There is a considerable amount of evidence suggesting that strand breaks are most likely to occur at the guanine site on the DNA strand [106, 134, 135, 136, 111]. In particular, Wang *et al* found that dissociation by the addition of electrons to the guanine base, results in significant numbers of single and double strand breaks [136], which is in agreement with the above results. Figure 26 shows that guanine will be deprotonated, whereas Figure 27 shows that the barrier for breaking the $C_{3'}$-$O_{3'}$ bond in deprotonated $dGMPH^-$ is only 19 kcal/mol and that the total free energy change upon reaction is approximately zero. The barrier for protonated $dAMPH^-$ is similar to that of $dGMPH^-$, and significantly lower than those of $dCMPH^-$ and $dTMPH^-$. In

other words, strand breaks appear to be more likely at the purine than the pyrimidine sites, which is consistent with the results of Zheng *et al* who observed that the extent of damage to short polynucleotide sequences (GCAT) was lower when guanine and adenine were absent.

4.4.2. Double strands. A QM/MM study of the molecular reorganisation of solvated DNA double strands was recently conducted by Cauet *et al* [142]. Calculations were performed on 12-mer DNA fragments where two nucleotides were modelled at the DFT-M06-2X level of theory (hybrid DFT-HF functional), and the rest of the molecule, the environment and the counterions were treated at a classical (AMBER) level. These authors found that attachment would occur on the sugar-phosphate backbone, and that the P-O and C-C bonds were more susceptible to cleavage than the C-O bonds. However, they did not rule out a transfer of energy to the C-O bond. Apart form the possible limitations of the QM/MM approach, a main difference between these simulations and those described above is that these calculations were performed for double-stranded DNA, while the previous work focused on single nucleotides. In double-stranded situations, the base is already hydrogen-bonded to the complementary base in the other strand. Therefore, to protonate it has to seize a proton from the other base, instead of from a water molecule. A suggestion of possible transfer to the C-O bond may provide an explanation for the confusion surrounding strand breaks in solution. In some experiments SSB yields are significantly increased by the inclusion of a water environment [136, 143], so it seems confusing that SSB barriers can be so much higher than in gas phase. The barriers being calculated, however, are reliant on predictions made in the gas phase. Cauet *et al* suggested that other bonds can perhaps break and contribute to SSB yields, especially in longer DNA fragments in solution. This idea remains poorly explored, but it is certainly an area for further study.

4.4.3. Amino acids. Another major component of the physiological environment is the amino acids. DNA is wrapped around histones (proteins) in chromatin and the close proximity of amino acids can influence the interaction between excess electrons and DNA in various ways. There have been both experimental and theoretical investigations focusing on the interactions of amino acids with DNA components, including hydrogen bonding, ionic and van der Waals interactions, and stacking and T-shaped interactions. Gas-phase studies have highlighted that a barrier-free proton transfer occurs between anionic nucleobases and amino acids [144]. Hydrogen bonds, in turn, have been shown to stabilise anionic nucleobase structures in an aqueous environment, which highlighted proton acceptor sites as particularly able to stabilise a structure [91]. Recently, Solomun and Skalický reported that the single strand DNA binding E. coli protein can effectively inhibit single strand breaks (SSB) of oligonucleotides induced by 3 eV LEEs [145]. Furthermore, Ptasińska *et al* reported the fragmentation of short DNA strands irradiated by a 1 eV electron beam in the presence of glycine and arginine [146]. Their results showed that DNA damage is promoted at low amino acid

concentrations and inhibited at high concentrations. It has been suggested that there are two underlying mechanisms influencing these findings. Firstly the protein may create a physical shielding to the DNA. In addition the hydrogen-bonding interactions may play an essential role in quenching SSB through the stabilization of the anionic species. These hypotheses were successively tested via FPMD simulations of a single thymine in a bath of 32 glycine molecules instead of water [147]. These were fully quantum simulations at the DFT-PBE level and TZVP-MOLOPT basis set.

In these simulations, after a short period dominated by proton transfer, a dynamical equilibrium was established between the canonical and zwitterionic versions of glycine and protonated and deprotonated versions of this molecule. When an excess electron was added, it initially finds itself in a pre-solvated state, that is delocalised over the the thymine and the glycine. What happens subsequently depends on the bonding pattern between thymine and glycine. A first possibility, which is shown in the right panel in Figure 28, occurs when the local environment of the thymine contains hydrogen-bonded glycine molecules that are ready to transfer a proton to the thymine. In this case, the excess electron is chemically stabilised in the nucleobase in a manner that is similar to the case observed for protonation from water discussed in Section 4.4.1. A second possibility

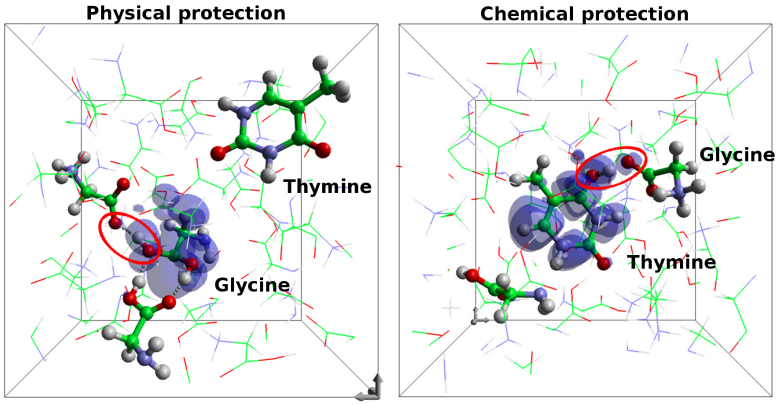

Figure 28. Snapshot of the spin density on the thymine-glycine complex with an excess electron after equilibration. Left panel: the electron is scavenged by one of the glycines. Right panel: the electron is localised on the thymine. In both cases the excess electron is stabilized by a proton transferred from a neighbouring glycine (red circles). Reproduced from Ref. [147] with permission from the Royal Society of Chemistry.

is that glycine, which has an electron affinity that is similar to that of the nucleobases, physically scavenges the excess electron and thus prevents it from causing damage to the DNA. This is shown in the left panel in Figure 28. Both of these mechanisms are protective of DNA and this study represents a first step towards including the most important components that surround DNA in the physiological medium and in understanding how natural selection has optimized the cellular medium so as to prevent DNA damage events. Further work in this direction is clearly needed.

5. Concluding remarks and future research avenues

There are two main ways by which radiation can cause damage to DNA: directly, by ionising DNA, and indirectly, by ionising the surrounding medium and generating reactive secondary species that go on to attack DNA. Which one is more important is subject to debate. It is estimated that two thirds of the damage can be attributed to indirect events [11, 12]. A thorough discussion of the role of of holes in direct DNA damage events can be found in [21]. Here we focused on indirect damage only. Within this context, the two main points to elucidate are: how does ionisation of the medium cause DNA damage, and which are the most relevant ionisation products in this respect. The two main ionisation products that are generated by the incident radiation are low-energy electrons and radicals. There are many interesting open questions around radicals, in particular their diffusion properties in the medium and the mechanisms via which they interact with DNA and cause damage [148]. Radical interactions with DNA are not only relevant in relation to radiation damage, but also central to metabolic damage, thus constituting an interesting avenue for research in its own right.

In this review we have limited ourselves to the study of the interactions of low-energy electrons with DNA, focusing on the endpoint effects of electron irradiation and leaving aside the so-called physical stage that describes the ionisation process and the inelastic transport of electrons through the medium. We have looked in detail at what happens when electrons are captured resonantly by DNA nucleobases, nucleotides, and larger fragments. In particular, we have described the theoretical and experimental investigations that have shown that resonances live long enough to form a transient negative ion that dissociates via the mechanism known as dissociative electron attachment, and that this mechanism is particularly prevalent when DNA is in an aqueous environment. To examine the dynamics after a DEA event we have used a model in which the excess electron energy is instantaneously transferred to a specific bond as vibrational energy. The main conclusion of these studies is that bond dissociation energies calculated in gas phase cannot be used to estimate the likelihood that a bond will break when the base or nucleotide is solvated. When molecules are solvated, breaking bonds requires a significantly greater input of energy as the surrounding water molecules can reflect energy back into the solute through caging effects. These processes bounce energy between the solute and the medium and thus serve to dissipate the vibrational energy that the DEA event transferred into the bond.

We thus assume that when the LEE is captured at high energy, the amount of energy that is transferred to the bond will be sufficiently large to break it. Furthermore, this large input of energy will allow the dissociated fragment to travel a great distance and this substantial motion will prevent the bond from reforming. When, by contrast, the LEE is captured at low energy, reflection and dissipation of energy will either prevent the bond from breaking at all or will prevent the DNA fragments that are formed when the bond breaks from moving apart. Consequently, when the LEE is captured at low energy the system will most likely settle down to an equilibrium configuration with the excess

electron occupying the SOMO and the DNA fragment remaining intact. In other words, the system will, upon attaching a very low energy electron to the DNA strand, relax into the ground state for the anion. It is important to note, however, that the work we have presented herein has been performed on single DNA bases and on single nucleotides. It is reasonable to suppose that these conclusions would also hold for longer DNA fragments but it is also important to remember that dealing with these larger systems introduces new questions. For example: if only one of the strands in a double-stranded geometry were to break, the two ends of the broken strand are prevented from moving apart by the hydrogen-bonds to the complementary strand. Whether or not this is one of the mechanisms that is used in the cell to repair damaged DNA remains unclear and could be a topic for further investigation.

The previous paragraph may make it sound like the simulations presented in this review have shown that, in aqueous environment and at room temperature, strand breaking cannot be triggered by DEA processes involving very low energy electrons. It is important to remember, however, that strand breaking reactions can occur in ground state anions and that the mechanism for such reactions relies on thermal activation. If this mechanism involving electron capture and relaxation to the ground state, followed by an activated process in which a weakened bond is broken, is dominant, then the rate at which strands are broken should be dependent on temperature.

In addition to studying the after effects of DEA we have also analysed electron affinities for DNA fragments in the gas-phase and in the presence of an aqueous environment that was modelled both explicitly and using a polarisable continuum. We concluded from these studies that solvation increases the electron affinity and that hydrogen-bonding plays a crucial role. We have also modelled bond breaking reactions that occur on the energy landscape of the ground state anion in a variety of different situations. These studies used constrained first-principles molecular dynamics simulations to compute free energy profiles and activation barriers. These calculated barriers were on the order of 20 kcal/mol, but they can increase or decrease depending on the environment. In particular, protonation of the base tends to raise the barriers and thus protects nucleotides against strand breaks. Future work in this direction would involve simulating larger fragments such as polynucleotides and double-stranded small fragments in order to determine if there are particular sequences of nucleobases that favour or inhibit strand breaking reactions. There are then open questions regarding how double strand breaks occur and what role the amino acids of the histones play in this process. We have shown that amino acids protect nucleobases by protonating them or by scavenging electrons. Whether or not this remains the case for nucleotides and larger fragments, and in models with a more accurate representation of chromatin is an open question, however.

In short, our understanding of the damage caused to DNA by low-energy electrons has come a long way since the first experiments in Sanche's group and new experiments and simulations continue to shed light into the matter. We have, however, only really dipped our toe into this vast problem. A colossal amount of work is still required until

we get a clear understanding into how DNA damage by LEE is achieved in physiological environments, in part because the cell contains enzymatic machinery that can interact with broken DNA and repair it [149]. In the meantime, this review suggests a number of open research avenues. Hopefully these will be explored in the near future.

Acknowledgments

We thank Maeve Smyth, Ilya Fabrikant, Lila Bouëssel du Bourg, Amy Williamson and Declan Scullion for their contributions to parts of this work. We also thank Michael Ferguson for help with the chemical drawings, and Pablo de Vera for creating figure 4 of the nucleosome. We have had numerous useful discussions with Fred Currell, Anil Kumar, Amitava Adhikary, Ilya Fabrikant and Leon Sanche for which we are grateful. Lastly we received computational support from the UK national high performance computing service, ARCHER via the UKCP consortium and funded by EPSRC grant ref EP/K013564/1.

[1] Boudaiffa B, Cloutier P, Hunting D, Huels M A and Sanche L 2000 Science **5458** 1658–60
[2] Koltzoff N K 1928 Biologisches Zentralblatt **48** 345–69
[3] Avery O T, Macleod C M and McCarty M 1944 J. Exp. Med. **79** 137–8
[4] Watson J D and Crick F H 1953 Nature **171** 737–8
[5] Friedberg E C 2003 Nature **421** 436–40
[6] Belau L, Wilson K R, Leone S R and Ahmed M 2007 J. Phys. Chem. A **111** 7562–8
[7] Dawley M M, Tanzer K, Cantrell W A, Plattner P, Brinkmann N R, Scheier P, Denifl S and Ptasinska S 2014 Phys. Chem. Chem. Phys. **16** 25039–53
[8] Page R H, Larkin R, Yhen Y R and Lee Y T 1988 J. Chem. Phys. **88** 2249
[9] IAEA: Radiation in everyday life. `https://www.iaea.org/Publications/Factsheets/English/radlife`. Accessed: 13-03-2017
[10] Lodge M, Pijls-Johannesma M, Stirk L, Munro A J, Ruysscher D D and Jefferson T 2007 Radiotherapy and Oncology **83** 110 – 122
[11] Alizadeh E and Sanche L 2012 Chemical Reviews **112** 5578–5602
[12] Jonah C and Rao B 2001 Radiation Chemistry: Present Status and Future Trends Studies in physical and theoretical chemistry (Elsevier) ISBN 9780444829023
[13] Nikjoo H, Uehara S, Emfietzoglou D and Brahme A 2008 New Journal of Physics **10** 075006
[14] Kallikragas D T, Plugatyr A Y and Svishchev I M 2013 J. Chem. Eng. Data **3** 1289
[15] Surdutovich E, Yakubovich A V and Solov'yov A V 2014 Scientific Reports **59** 1964–9
[16] de Vera P, Mason N J, Currell F J and Solov'yov A V 2016 Eur. Phys. J. D **70** 183
[17] Lewis F D, Liu X, Liu J, Miller S E, Hayes R T and Wasielewski M R 2000 Nature **406** 51–53
[18] Giese B, Amaudrut J, Kohler A K, Sporran M and Wessely S 2001 Nature **412** 318–320
[19] Conwell E M and Rakhmanova S V 2000 Proc. Natl. Acad. Sci. USA **97** 4556–60
[20] Shao F, O'Neill M A and Barton J K 2004 Proc. Natl. Acad. Sci. USA **101** 17914–9
[21] Yun B H, Lee Y A, Kim S K, Kuzmin V, Kolbanovskiy A, Dedon P C and Shafirovich V 2007 J. Am. Chem. Soc. **129** 9321–32
[22] Livshits G I, Stern A, Rotem D, Borovok N, Eidelshtein G, Migliore A, Penzo E, Wind S J, di Felice R, Skourtis S S, Cuevas J C, Gurevich L, Kotlyar A B and Porath D 2014 Nature Nanotechnology **9** 1040–6
[23] Pimblott S M and La Verne J A 2007 Radiat. Phys. Chem. **76** 1244–7
[24] Steenken S 1989 Chemical Reviews **89** 503–520
[25] Kumar A, Adhikary A, Shamoun L and Sevilla M D 2016 The Journal of Physical Chemistry B **120** 2115–2123
[26] von Sonntag C 1987 The chemical basis of radiation biology (Taylor and Francis)
[27] Breen A P and Murphy J A 1995 Free Radical Biology and Medicine **18** 1033–77
[28] Alizadeh E, Sanz A G, Garcia G and Sanche L 2013 J. Phys. Chem. Lett. **4** 820–825
[29] Haxton D J, Zhang Z, Meyer H D, Rescigno T N and McCurdy C W 2004 Phys. Rev. A **69** 062714
[30] Sanche L 2009 Low-Energy Electron Interaction with DNA: Bond Dissociation and Formation of Transient Anions, Radicals and Radical Anions, Radicals in Nucleic Acids (Hoboken, NJ: Wiley) pp 239–294
[31] Arumainayagam C R, Lee H, Nelson R B, Haines D R and Gunawardane R 2010 Surf. Sci. Rep. **65** 1–44
[32] Baccarelli I, Bald I, Gianturco F, Illenberger E and Kopyra J 2011 Physics Reports **508** 1–44
[33] Alizadeh E, Orlando T and Sanche L 2015 Annu. Rev. Phys. Chem. **66** 379–398
[34] Kumar A and Sevilla M 2012 Low energy electron (LEE) induced DNA damage: Theoretical approaches to modeling experiment Handbook of Computational Chemistry Vol. III: Applications – Biomolecules ed Shukla M and Leszczynski J (Dodrecht, Netherlands: Springer) pp 1215–1256
[35] Caron L and Sanche L 2012 Theoretical studies of electron interactions with dna and its subunits: from tetrahydrofuran to plasmid dna Low-Energy Electron Scattering from Molecules,

Biomolecules and Surfaces ed Čársky P and Čurik R (Boca Raton, FL: Taylor & Francis)
[36] Gu J, Leszczynski J and Schaefer H I 2012 Chem. Rev. **112** 5603–5640
[37] Cobut V, Frongillo Y, Patau J P, Goulet T, Fraser M J and Jay-Gerin J P 1998 Radiation Physics and Chemistry **51** 229–243
[38] Singh N P, McCoy M T, Tice R R and Schneider E L 1988 Experimental Cell Research **175** 184–191
[39] Luo X, Zheng Y and Sanche L 2014 Journal of Chemical Physics **140** 155101
[40] Russo N, Toscano M and Grand A 2000 Journal of Computational Chemistry **21** 1243–1250
[41] Barrios R, Skurski P and Simons J 2002 Journal of Physical Chemistry B **106** 7991–7994
[42] Martin F, Burrow P D, Cai Z L, Cloutier P, Hunting D and Sanche L 2004 Physical Review Letters **93** 068101
[43] Huels M, Hahndorf I, Illenberger E and Sanche L 1998 Journal of Chemical Physics **108** 1309–1312
[44] Fisher D J and Zhang C 1994 Journal of Applied Physics **76** 606–608
[45] Christophorou L and Olthoff J 2012 Fundamental Electron Interactions with Plasma Processing Gases Physics of Atoms and Molecules (Springer US) ISBN 9781461347415
[46] Denifl S, Ptasinska S, Cingel M, Matejcik S, Scheier P and Märk T 2003 Chemical Physics Letters **377** 74–80
[47] Hanel G, Gstir B, Denifl S, Scheier P, Probst M, Farizon B, Farizon M, Illenberger E and Märk T D 2003 Phys. Rev. Lett. **90** 188104
[48] Gohlke S, Abdoul-Carime H and Illenberger E 2003 Chemical Physics Letters **380** 595–599
[49] Abdoul-Carime H, Gohlke S and Illenberger E 2004 Physical Review Letters **92** 168103
[50] Ptasinska S, Denifl S, Grill V, Mark T D, Illenberger E and Scheier P 2005 Phys. Rev. Lett. **95** 093201
[51] Ptasinska S, Denifl S, Scheier P, Illenberger E and Mark T 2005 Angewandte Chemie - International Edition **44** 6941–6943
[52] Ibanescu B C and Allan M 2009 Physical Chemistry Chemical Physics **11** 7640–7648
[53] Čársky P and Čurik R (eds) 2016 Low-Energy Electron Scattering from Molecules, Biomolecules and Surfaces (Boca Raton, FL: CRC Press, Taylor & Francis) ISBN 9781439839119
[54] Tennyson J 2010 Physics Reports **491** 29–76
[55] Fabrikant I 1991 Physical Review A **43** 3478–3486
[56] Domcke W 1991 Phys. Rep. **208** 97–188
[57] McCurdy C, Isaacs W, Meyer H D and Rescigno T 2003 Phys. Rev. A **67** 042708–19
[58] Caron L and Sanche L 2003 Physical Review Letters **91** 1132011–1132014
[59] Caron L, Sanche L, Tonzani S and Greene C H 2008 Phys. Rev. A **78** 042710
[60] Gallup G and Fabrikant I 2011 Physical Review A **83** 012706
[61] Nesbet R 1981 Physical Review A **24** 1184–1193
[62] Hotop H, Ruf M W, Allan M and Fabrikant I 2003 Adv. At. Mol. Opt. Phys. **49** 86216
[63] Smyth M, Kohanoff J and Fabrikant I 2014 Journal of Chemical Physics **140** 184313
[64] Bald I, Kopyra J and Illenberger E 2006 Angewandte Chemie - International Edition **45** 4851–4855
[65] Baccarelli I, Gianturco F, Grandi A, Sanna N, Lucchese R, Bald I, Kopyra J and Illenberger E 2007 Journal of the American Chemical Society **129** 6269–6277
[66] Bald I, Flosadettir H D, Kopyra J, Illenberger E and Ingelfsson O 2009 International Journal of Mass Spectrometry **280** 190–197
[67] Abdoul-Carime H, Gohlke S, Fischbach E, Scheike J and Illenberger E 2004 Chemical Physics Letters **387** 267–270
[68] Ptasinska S, Denifl S, Gohlke S, Scheier P, Illenberger E and Mark T 2006 Angewandte Chemie - International Edition **45** 1893–1896
[69] Konig C, Kopyra J, Bald I and Illenberger E 2006 Phys. Rev. Lett. **97** 018105
[70] Burrow P, Gallup G and Modelli A 2008 Journal of Physical Chemistry A **112** 4106–4113
[71] Bald I, Dabkowska I and Illenberger E 2008 Angewandte Chemie - International Edition **47**

8518–8520
[72] Bao X, Wang J, Gu J and Leszczynski J 2006 Proceedings of the National Academy of Sciences of the USA **103** 5658–5663
[73] Simons J 2006 Accounts of Chemical Research **39** 772–779
[74] Dora A, Bryjko L, van Mourik T and Tennyson J 2012 Journal of Physics B: Atomic, Molecular and Optical Physics **45** 175203
[75] Dora A, Bryjko L, Van Mourik T and Tennyson J 2012 Journal of Chemical Physics **136** 024324
[76] Sieradzka A and Gorfinkiel J 2017 J. Chem. Phys. (under review)
[77] Fabrikant I, Eden S, Mason N and Fedor J 2017 Adv. At. Mol. Opt. Phys. (in press)
[78] Görling A 1996 Phys. Rev. A **54** 3912–3915
[79] Kohanoff J 2006 Electronic Structure Calculations for Solids and Molecules: Theory and Computational Methods (Cambridge, UK: CUP) ISBN 9780521815918
[80] van Faassen M, Wasserman A, Engel E, Zhang F and Burke K 2007 Phys. Rev. Lett. **99** 043005
[81] Rizzi V, Todorov T N, Kohanoff J J and Correa A A 2016 Phys. Rev. B **93** 024306
[82] Trani F, Scalmani G, Zheng G, Carnimeo I, Frisch M J and Barone V 2011 Journal of Chemical Theory and Computation **7** 3304–3313
[83] Negre C F A, Fuertes V C, Oviedo M B, Oliva F Y and S?nchez C G 2012 The Journal of Physical Chemistry C **116** 14748–14753
[84] Correa A A, Kohanoff J, Artacho E, Sánchez-Portal D and Caro A 2012 Phys. Rev. Lett. **108** 213201
[85] Horsfield A P, Bowler D R, Fisher A J, Todorov T N and S?nchez C G 2005 Journal of Physics: Condensed Matter **17** 4793
[86] McEniry, E J, Wang, Y, Dundas, D, Todorov, T N, Stella, L, Miranda, R P, Fisher, A J, Horsfield, A P, Race, C P, Mason, D R, Foulkes, W MC and Sutton, A P 2010 Eur. Phys. J. B **77** 305–329
[87] Rajam A K, Raczkowska I and Maitra N T 2010 Phys. Rev. Lett. **105** 113002
[88] Tully J C 1990 The Journal of Chemical Physics **93** 1061–1071
[89] Rizzi V, Todorov T N and Kohanoff J J 2017 Scientific Reports **(in press)**
[90] Hutter J, Iannuzzi M, Schiffmann F and VandeVondele J 2014 Wiley Interdisciplinary Reviews: Computational Molecular Science **4** 15–25
[91] Smyth M and Kohanoff J 2011 Physical Review Letters **106** 238108
[92] Kočišek J, Pysanenko A, Farnik M and Fedor J 2016 The Journal of Physical Chemistry Letters **7** 3401–3405
[93] Berg J M, Tymoczko J L and Stryer L 2002 Biochemistry, Fifth Edition: International Version (W. H. Freeman) ISBN 978-0-7167-4684-3
[94] Kumar A, and Sevilla M D 2007 The Journal of Physical Chemistry B **111** 5464–5474
[95] Kumar A and Sevilla M 2009 ChemPhysChem **10** 1426–1430
[96] Steenken S 1992 Free Radical Research Communications **16** 349–379
[97] Liu B, Nielsen S B, Hvelplund P, Zettergren H, Cederquist H, Manil B and Huber B A 2006 Phys. Rev. Lett. **97** 133401
[98] Gu J, Xie Y and Schaefer H F 2007 Nucleic Acids Research **35** 5165–5172
[99] Gu J, Xie Y and Schaefer III H 2010 The Journal of Physical Chemistry B **114** 1221–1224
[100] Haranczyk M, Gutowski M, Li X and Bowen K 2007 Journal of Physical Chemistry B **111** 14073–14076
[101] Kim S, Wheeler S E and Schaefer H F 2006 The Journal of Chemical Physics **124** 204310
[102] Kim S and Schaefer H 2006 Journal of Chemical Physics **125** 144305
[103] Dedikova P, Neogrady P and Urban M 2011 The Journal of Physical Chemistry A **115** 2350–2358
[104] Smets J, McCarthy W and Adamowicz L 1996 Chemical Physics Letters **256** 360–369
[105] Gu J, Wang J and Leszczynski J 2006 Journal of the American Chemical Society **128** 9322–9323
[106] Gu J, Wang J and Leszczynski J 2010 Nucleic Acids Research **38** 5280–5290
[107] Gu J, Wang J and Leszczynski J 2011 Journal of Physical Chemistry B **115** 14831–14837
[108] Schyman P, Laaksonen A and Hugosson H 2008 Chemical Physics Letters **462** 289–294

[109] Li Z, Cloutier P, Sanche L and Wagner J R 2010 Journal of the Americal Chemical Society **132** 5422–5427
[110] Dinh P M, du Bourg L B, Gao C Z, Gu B, Lacombe L, McAllister M, Smyth M, Tribello G, Vincendon M, Kohanoff J, Reinhard P G, Sanche L and Suraud E 2017 On the Quantum Description of Irradiation Dynamics in Systems of Biological Relevance (Cham: Springer International Publishing) pp 277–309
[111] Zheng Y, Wagner J and Sanche L 2006 Physical Review Letters **96** 208101
[112] Ptasinska S and Sanche L 2007 Phys. Chem. Chem. Phys. **9** 1730–1735
[113] Zheng Y, Cloutier P, Hunting D, Sanche L and Wagner J 2005 Journal of the American Chemical Society **127** 16592–16598
[114] Gu J, Xie Y, and Schaefer III H F 2006 Journal of the American Chemical Society **128** 1250–1252
[115] Berdys J, Anusiewicz I, Skurski P and Simons J 2004 Journal of Physical Chemistry A **108** 2999–3005
[116] Svozil D, Jungwirth P and Havlas Z 2004 Collection of Czechoslovak Chemical Communications **69** 1395–1428
[117] Schiedt J, Weinkauf R, Neumark D and Schlag E 1998 Chemical Physics **239** 511–524
[118] Desfrancois C, Periquet V, Bouteiller Y and Schermann J 1998 Journal of Physical Chemistry A **102** 1274–1278
[119] Colson A O, Besler B and Sevilla M 1992 Journal of Physical Chemistry **96** 9787–9794
[120] Roca-Sanjuan D, Merchan M, Rubio M and Serrano-Andres L 2008 Journal of Chemical Physics **129** 095104
[121] Riley K, Op't Holt B and Merz Jr K 2007 Journal of Chemical Theory and Computation **3** 407–433
[122] Wesolowski S S, Leininger M L, Pentchev P N and Schaefer III H F 2001 Journal of the American Chemical Society **123** 4023–4028
[123] Sarmah P and Deka R C 2008 Molecular Simulation **34** 879–885
[124] Becke A 1993 The Journal of Chemical Physics **98** 5648–5652
[125] Lee C, Yang W and Parr R 1988 Physical Review B **37** 785–789
[126] Zhao Y, Schultz N and Truhlar D 2006 Journal of Chemical Theory and Computation **2** 364–382
[127] Zhao Y and Truhlar D 2008 Theoretical Chemistry Accounts **120** 215–241
[128] Smyth M 2012 A Computational Study of Radiation Damage to DNA Ph.D. thesis Queen?s University Belfast
[129] Chen E and Chen E 2000 Journal of Physical Chemistry B **104** 7835–7844
[130] Matthew J and Richards F 1984 Biopolymers **23** 2743–2759
[131] Sponer J, Burda J, Sabat M, Leszczynski J and Hobza P 1998 Journal of Physical Chemistry A **102** 5951–5957
[132] Mennucci B 2012 Wiley Interdisciplinary Reviews: Computational Molecular Science **2** 386–404
[133] Ptasinska S and Sanche L 2007 Physical Review E - Statistical, Nonlinear, and Soft Matter Physics **75** 031915
[134] Schyman P and Laaksonen A 2008 Journal of the American Chemical Society **130** 12254–12255
[135] Gu J, Wang J and Leszczynski J 2010 ChemPhysChem **11** 175–181
[136] Wang C R, Nguyen J and Lu Q 2009 Journal of the American Chemical Society **131** 11320–11322
[137] Uhlig F, Marsalek O and Jungwirth P 2012 The Journal of Physical Chemistry Letters **3** 3071–3075
[138] Smyth M and Kohanoff J 2012 Journal of the American Chemical Society **134** 9122–9125
[139] McAllister M, Smyth M, Gu B, Tribello G A and Kohanoff J 2015 The Journal of Physical Chemistry Letters **6** 3091–3097
[140] McAllister M 2012 Computational Modelling of Radiation Damage to DNA Ph.D. thesis Queen?s University Belfast
[141] Steenken S, Telo J, Novais H and Candeias L 1992 Journal of the American Chemical Society **114** 4701–4709

[142] Cauet E, Bogatko S, Livin J, De Proft F and Geerlings P 2013 Journal of Physical Chemistry B **117** 9669–9676
[143] Ito T, Baker S, Stickley C, Peak J and Peak M 1993 International Journal of Radiation Biology **63** 289–296
[144] Szyperska A, Gajewicz A, Mazurkiewicz K, Leszczynski J and Rak J 2011 Phys. Chem. Chem. Phys. **13** 19499–19507
[145] Solomun T and Skalicky T 2008 Chemical Physics Letters **453** 101–104
[146] Ptasinska S, Li Z, Mason N J and Sanche L 2010 Phys. Chem. Chem. Phys. **12** 9367–9372
[147] Gu B, Smyth M and Kohanoff J 2014 Phys. Chem. Chem. Phys. **16** 24350–24358
[148] Wu Y, Mundy C J, Colvin M E and Car R 2004 The Journal of Physical Chemistry A **108** 2922–2929
[149] Banerjee A, Yang W, Karplus M and Verdine G L 2005 Nature **434** 612–618